

AN AB INITIO SURFACE STUDY OF FeTi FOR
HYDROGEN STORAGE APPLICATIONS

A THESIS SUBMITTED TO
THE GRADUATE SCHOOL OF NATURAL AND APPLIED SCIENCES
OF
MIDDLE EAST TECHNICAL UNIVERSITY

BY

AFSHIN IZANLOU

IN PARTIAL FULFILLMENT OF THE REQUIREMENTS
FOR
THE DEGREE OF MASTER OF SCIENCE
IN
METALLURGICAL AND MATERIALS ENGINEERING

SEPTEMBER 2009

Approval of the thesis:

**AN AB INITIO SURFACE STUDY OF FeTi FOR
HYDROGEN STORAGE APPLICATIONS**

submitted by **AFSHIN IZANLOU** in partial fulfillment of the requirements for the degree of **Master of Science in Metallurgical and Materials Engineering, Middle East Technical University** by

Prof.Dr. Canan Özgen
Dean, Graduate School of **Natural and Applied Sciences** _____

Prof.Dr. Tayfur Öztürk
Head of Department, **Metallurgical and Materials Engineering** _____

Prof.Dr. M. Kadri Aydınol
Supervisor, **Metallurgical and Materials Engineering Dept., METU** _____

Examining Committee Members:

Prof.Dr. Tayfur Öztürk
Metallurgical and Materials Engineering Dept., METU _____

Prof.Dr. M. Kadri Aydınol
Metallurgical and Materials Engineering Dept., METU _____

Prof.Dr. İshak Karakaya
Metallurgical and Materials Engineering Dept., METU _____

Prof.Dr. Mehmet Parlak
Physics Dept., METU _____

Assist. Prof.Dr. Emrah Ünalın
Metallurgical and Materials Engineering Dept., METU _____

Date:

_____ 11.09.2009

I hereby declare that all information in this document has been obtained and presented in accordance with academic rules and ethical conduct. I also declare that, as required by these rules and conduct, I have fully cited and referenced all material and results that are not original to this work.

Name, Last Name : AFSHIN, IZANLOU

Signature :

ABSTRACT

AN AB INITIO SURFACE STUDY OF FeTi FOR HYDROGEN STORAGE APPLICATIONS

IZANLOU, Afshin

M.S., Department of Metallurgical and Materials Engineering

Supervisor: Prof. Dr. M. Kadri Aydınol

September 2009, 51 pages

In this study, the effect of surface crystallography on hydrogen molecule adsorption properties on FeTi surfaces is presented. Furthermore, the substitutional adsorption of 3d-transition metals on (001), (110) and (111) surfaces of FeTi is studied. Using ab initio pseudopotential methods, the adsorption energies of hydrogen and 3d-transition metals are calculated. In substitutional adsorption of 3d-transition metals, Fe-terminated (111) and Ti-terminated (001) surfaces, are found to express the lowest adsorption energies. The adsorption energy versus adsorbed elements' curves are very alike for all the surfaces. According to this, going from the left to right of periodic table, the adsorption energies increase first. The maximum energy belongs to Cr, Mn and Fe for all the surfaces. Then a minimum is observed in Co for all the surfaces and after that the energy increases again. Adsorption energies of atomic and molecular hydrogen are calculated on high symmetry sites of surfaces. As a result, top and bridge sites came out to be the most stable positions for molecular and atomic hydrogen adsorption, respectively, for (001) and (111) surfaces in all terminations. In (110) surface; however, 3-fold (Ti-Ti)_L-Fe and 3-fold (Ti-Ti)_S-Fe hollow sites express the lowest adsorption energies for molecular and atomic hydrogen, respectively. Considering the minimum adsorption energy sites for hydrogen molecule and atom, a path of dissociation of hydrogen molecule on surfaces is represented. After that by fully relaxing the hydrogen molecule on the surface and using CI-NEB method the activation energy for hydrogen dissociation is calculated. So it has been found that on Fe-

terminated (111) and FeTi (110) surfaces the dissociation of hydrogen molecule happens without activation energy. Meanwhile, the activation energy for Fe-terminated (001) surface and Ti-terminated (001) surface, is calculated to be 0.178 and 0.190 eV, respectively.

Keywords: FeTi Hydride, Hydrogen Storage, Ab Initio, Surface Adsorption.

ÖZ

FeTi BİLEŞİĞİNDE HİDROJEN DEPOLAMA UYGULAMALARI İÇİN TEMEL PRENSİPLER YÖNTEMİYLE YÜZEY ÇALIŞMASI

IZANLOU, Afshin

Yüksek Lisans, Metalurji ve Malzeme Mühendisliği Bölümü

Tez Yöneticisi: Prof. Dr. M. Kadri Aydınol

Eylül 2009, 51 sayfa

Bu çalışmada, FeTi bileşiğindeki yüzey kristalografisinin, hidrojen atom ve molekülünün soğrulmasına olan etkileri incelenmiştir. Ayrıca 3d geçiş metallerinin, FeTi bileşiğindeki düşük indisli yüzeylere yerine-geçen tip soğrulması da çalışılmıştır. Her iki çalışmada da irdelenen yüzeyler (001), (111) ve (110) kristal düzlemlerdir. Temel prensipler psödopotansiyel yöntemi kullanılarak hidrojen ve geçiş elementlerinin soğurma enerjileri hesap edilmiştir. Geçiş elementlerinin yerine-geçen tip soğurma enerjilerine bakıldığında, en düşük soğurma enerjilerinin Fe ile sonlanmış (111) yüzeyinde, daha Ti ile sonlanmış (001) yüzeyinde olduğu görülmüştür. Diğer yüzeylerdeki soğurma enerjileri bir birine yakın bir davranış sergilerken, en yüksek değerler Ti ile sonlanmış (111) yüzeyinde görülmüştür. Erken geçiş elementlerinden orta elementlere doğru gittikçe, soğurma enerjilerinde önce bir miktar artış olduğu görülmektedir. Bütün yüzeyler dikkate alındığında, bu artışın en fazla olduğu elementlerin Cr, Mn ve Fe olduğu, sonra Co elementine geldiğinde soğurma enerjisinin aniden düştüğü belirlenmiştir. Geç geçiş elementlerine doğru soğurma enerjileri tekrar bir artış göstermektedir. Hidrojen atomu ve molekülü soğurma enerjileri, bahsi geçen yüzeylerde yüksek simetriye sahip bir takım özel pozisyonlarda hesap edilmiştir. Buna göre, Fe ve Ti ile sonlanmış (001) ve (111) yüzeylerinde, H₂ molekülünün en düşük soğurma enerjisine sahip olduğu pozisyonun, yüzey atomlarının tepe noktası olduğu, H atomunda ise yüzey atomları arası köprü pozisyonu olduğu tespit edilmiştir. (110) yüzeyinde ise, H₂ molekülünün iki uzun köprülü

Ti ve bir Fe atomunun oluşturduđu üçlünün orta boşluđunu tercih ettiđi, H atomunun ise iki kısa köprülü Ti ve bir Fe atomunun oluşturduđu üçlünün orta boşluđuna sođrulduđu görölmüştür. En düşük sođurma enerjilerine sahip olan durumların analizi ile, her bir yüzey için, H₂ molekülü için ayrışma mekanizmaları ileri sürölmüştür. Bu mekanizmaları dikkate alınarak, hidrojenin ayrışma reaksiyonunun aktivasyon enerjileri hesap edilmiştir. Buna göre, Fe ile sonlanmış (111) ve (110) yüzeylerinde ayrışmanın aktivasyon içermediđi tespit edilmiştir. Ancak her bir H₂ molekülünün ayrışması için, Fe ile sonlanmış (001) yüzeyinde 0.178 eV ve Ti ile sonlanmış (001) yüzeyinde 0.190 eV aktivasyon engeli olduđu bulunmuştur.

Anahtar kelimeler: FeTi hidrür, Hidrojen depolama, Temel prensipler yöntemi, Yüzey sođurulması.

ACKNOWLEDGEMENTS

I would like to thank my supervisor, Prof.Dr. Kadri Aydınol, whom helped me alot during my master thesis. I also thank my family whom supported me with their ultimate kindness.

TABLE OF CONTENTS

ABSTRACT.....	iv
ÖZ.....	vi
ACKNOWLEDGEMENTS.....	viii
TABLE OF CONTENTS.....	ix
CHAPTERS	
1 INTRODUCTION	1
1.1 Hydrogen energy.....	1
1.2 Hydrogen storage.....	3
1.2.1 Hydrogen storage in hydrides	5
1.3 First principles studies	10
1.3.1 Ab initio studies on hydrides	11
1.3.2 Ab initio studies on adsorption	13
2 METHODOLOGY	16
2.1 Bulk calculations.....	16
2.2 Surface calculations	18
2.2.1 Pure surfaces	18
2.2.2 Alloyed surfaces.....	23
3 RESULTS and DISCUSSIONS.....	26
3.1 Pure surfaces	26
3.1.1 Surface structure, relaxation and reconstruction	26
3.1.2 Hydrogen adsorption energies	28
3.2 Alloyed surfaces.....	36

3.2.1 Surface structure, relaxation and reconstruction.....	36
3.2.2 Substitutional adsorption energy of alloying elements	44
4 CONCLUSIONS	47
REFERENCES	49

To Stewie Griffin

CHAPTER 1

INTRODUCTION

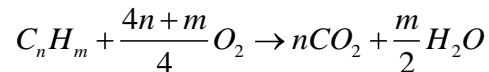
1.1 Hydrogen energy

Hydrogen is a versatile energy carrier and can be used in a variety of ways. In future, it could potentially replace petroleum products. The utilization of hydrogen as energy source on a sizable scale involves five basic issues: production, storage and transport, application, safety and economy [1].

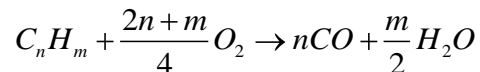
Hydrocarbons are the main source for the production of hydrogen on an industrial scale. The many production routes for hydrogen; however, are by no means of equal economic importance. Most of the hydrogen for industrial use is produced from natural gas and oil, either as a main product or as a byproduct from a process involving a chemical conversion. In many cases the chemical processes releasing hydrogen are intermediate steps in a large process chains. These main reactions can be summarized by the general term gasification. Principally, hydrogen can be extracted from any hydrocarbon. Accordingly, the number of possible raw materials is large: coal, heavy oil, light oil, methane and biomass [2].

Hiller and Reimert [3] classify gasification reactions into 4 groups:

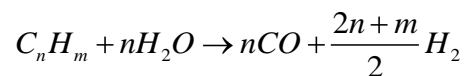
1) reaction with molecular oxygen or combustion:



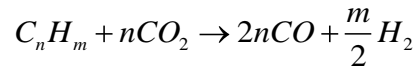
and for partial combustion of hydrocarbons to carbon monoxide and steam,



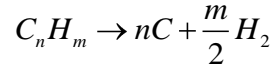
2) reactions with steam or homogeneous water gas reaction:



3) reaction with carbon dioxide:



4) soot reactions or decomposition of hydrocarbons:



Water, a huge resource on earth, can be split into its constituents hydrogen and oxygen by means of electrical energy. This process is called water electrolysis. In all different technologies for water electrolysis, the underlying general process is the same: water is supplied to an electrochemical cell where hydrogen evolves at the cathode and oxygen at the anode when supplied with a sufficiently high voltage level. Ions are transported through an electrolyte and a membrane ensures the separation of the two evolving gases.

Hino and Yan in their research [4] present hydrogen production from nuclear energy. Hydrogen production from water using nuclear energy offers one of the most attractive zero-emission energy strategies. It is the only one that is practical on a substantial scale including high-temperature gas-cooled reactor and very high temperature reactor. Nuclear energy can produce hydrogen in several ways: (1) nuclear heated steam reforming of natural gas, (2) electrolysis of water using nuclear power, (3) high-temperature electrolysis of steam using minor heat and major electricity from nuclear reactor, and (4) thermochemical splitting of water using major heat and minor electricity from the nuclear reactor.

Bechrakis and Varkaraki [5] study hydrogen production from wind energy. This process is, more precisely, the hydrogen production by the electrolysis of water, where the main power input is electrical power produced from the conversion of wind energy. As a concept, it is a very promising way to produce hydrogen. It is not only because the fact that both procedures are renewable and nonpolluting, but also because wind energy conversion systems can become more effective by incorporating an energy storage medium with such a versatile energy carrier.

Dhere and Bennur [6] have investigated on the use of solar energy to produce hydrogen. There are two principal methods for the electrolysis of water to generate hydrogen viz active, that is, photo-assisted and non photo-assisted (passive or dark). The active method consists of utilization of photo-generated charge carriers in the electrolysis of water and other products. In the passive method, the electrolysis is carried out in the dark at low temperatures using an alkaline electrolyte at intermediate temperatures and oxide electrolytes at high temperatures.

De Jong [7] presents sustainable hydrogen production by thermomechanical biomass processing. Biomass as the source of hydrogen production is considered to be a leading practical and viable option for the near and mid-term future. A variety of biomass resources can be converted for energy supply. They can be divided into four general categories: (1) energy crops, (2) agricultural residues and wastes, (3) forestry waste and residues, and (4) industrial and municipal wastes.

Damle [8] studies hydrogen separation and purification. He indicates three technologies which have been most commonly used for separating hydrogen from synthesis gas: (1) adsorption of gas species other than hydrogen, which produces pure hydrogen as a product, (2) polymeric membranes, which offer bulk separation of hydrogen, and (3) cryogenic separation, which can provide multiple pure products.

1.2 Hydrogen storage

One of the concerns about the successful harnessing of hydrogen as energy source is generally associated with its storage and transportation. These problems are more and less related to the lightness and chemical activity of free hydrogen. As regards storage, hydrogen can be stored for use as energy source, in the following ways: gaseous storage, liquid storage, metal hydride storage, micro balloon storage and underground storage [1].

The hydrogen molecule can be found in various forms, depending on the temperature and the pressure, which are shown in the phase diagram, Fig. (1.1). The most common storage systems are high pressure gas cylinders with a maximum pressure of 20 MPa. New lightweight composite cylinders have been developed which are able to withstand pressures up to 80 MPa and so the hydrogen can reach a volumetric density of 36 kgm⁻³, approximately half that in its liquid form at the normal boiling point. The gravimetric H₂ density decreases with increasing pressure due to the increasing thickness of the walls of the pressure cylinder [2].

Liquid hydrogen is stored in cryogenic tanks at 21.2 K at ambient pressure. Due to low critical temperature of hydrogen (33 K) liquid hydrogen can only be stored in open systems, because there is no liquid phase existent above the critical temperature. The challenges of liquid hydrogen storage are the energy efficient liquefaction process and the thermal insulation of the cryogenic store vessel in order to reduce the hydrogen boil-off [2].

Gao and Krishnamurthy [9] gather information about some preliminary results that have been reported in the literature where a mixture of hydrogen with liquid nitrogen demonstrated substantially high densities at higher temperatures. This demonstrates some

simpler solutions to vehicular hydrogen storage. Such mixtures combined with a cryo-compressed vessel design may provide an optimal solution for hydrogen storage.

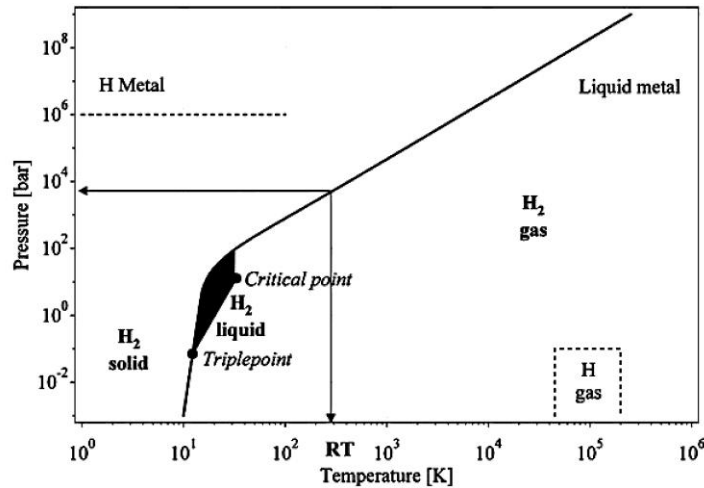


Figure 1.1 Phase diagram for hydrogen [2].

Carbon materials are very attractive candidates for hydrogen storage because of an ensemble of advantages like high specific surface area, microporosity, low mass and good adsorption ability. Activated carbon, because of its production process, has a very porous structure with a high specific surface area (from 1000 to 3000 m²g⁻¹) and considered to be the best carbonaceous adsorbent for hydrogen storage based on physisorption. Single wall carbon nanotubes exhibit a large free volume inside the tube and apart from this, the curvature of the graphene sheet and channels between the tubes in a bundle can be sites for new interactions with hydrogen. Large hydrogen storage in multi-walled carbon nanotubes between different concentric tubes seems to be impossible since then the strong carbon-carbon bond of the graphite sheets has to be stretched [2]. Pant and Gupta in their work [10] conclude that low storage capacity (about 3 wt%) and high cost of carbon nanotubes for building storage devices on a mass scale, are the main drawbacks of carbon materials. However, fast adsorption/desorption kinetics that is needed in practical applications is an advantage of carbon materials.

Zeolites, because of their attractive properties, have been intensively investigated for hydrogen adsorption capacities. They have a very open microporous structure with different framework types and high specific surface area. But very low hydrogen storage capacity (around 1 wt%) has been reported for different types of zeolites [2].

Metal-Organic Frameworks are a new wide class of extremely porous polymeric structures which consist of metal ions linked together through organic ligands. Of particular interest is the crystallites synthesized by Li et. al. [11] which are called nanocubes. Because of their apparently extraordinary properties, these porous materials have been studied with regard to their hydrogen storage capacity. Again, the storage capacities of these materials are not really considerable in ambient temperature and pressure [2].

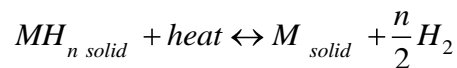
1.2.1 Hydrogen storage in hydrides

An alternative and promising means of storing hydrogen is in hydride compounds. Certain metals and their alloys, namely, magnesium-nickel, magnesium-copper and iron-titanium are capable of absorbing hydrogen gas to form chemical compounds referred to as hydrides. Such hydrogen storing method, avoids having to contain large volumes of hydrogen as gas or to maintain special pressures and temperatures needed for storing hydrogen as a compressed gas or as a liquid. On the other hand, research and development efforts are still required to investigate lighter hydrides or hydrides with even larger storage capacities which could lead to convenient use of hydrogen for different applications [1].

Metals, intermetallic compounds and alloys generally react with hydrogen and form mainly solid metal-hydrogen compounds. Hydrides exist as ionic, polymeric covalent, volatile covalent and metallic hydrides. Based on the strength of the bonds, metal and intermettalic hydrides are broadly classified into two categories: (1) reversible and (2) irreversible. Examples of reversible intermetal hydrides are as follows:

1. AB_5 is most common (e.g., nickel-metal hydride batteries with 1-1.25 reversible wt% capacity)
2. AB_2 very common (1.3 reversible wt% capacity)
3. AB (e.g., with 1.5 reversible wt% capacity)
4. A_2B (e.g., with 3.3-7.0 reversible wt% capacity)
5. AB_3 and A_2B_7

The reversible metal hydrides can undergo a reversible reaction as follows:



where the forward reaction is the release of hydrogen (or desorption) and the backward reaction is the adsorption of hydrogen (or charging). Reversible hydrides have been used for a long time in hydride-based batteries. These hydrides, such as $LaNi_5H_6$ or $FeTiH$, are typical low-temperature hydrides, that is, they have a dissociation pressure higher than 0.1

MPa at room temperature. In contrast, most of the light metal binary hydrides work at high temperatures. The light alkali metal hydrides such as LiH and NaH are more stable than MgH₂, with decomposition temperatures exceeding 500 °C [10].

The demarcation between the various types of hydrides is not sharp, they merge into each other according to the electronegativity of the elements concerned. The binary hydrides of the transition metals are predominantly metallic in character and are usually referred to as metallic hydrides. The lattice structure is that of a typical metal with atoms of hydrogen on the interstitial sites. This type of structure has the limiting compositions MH, MH₂ and MH₃. The hydrogen atoms fit into tetrahedral or octahedral holes in the metal lattice, or into a combination of the two types. Many of these compounds (MH_n) show large deviations from ideal stoichiometry (n=1,2,3) and can exist as multiphase systems. Especially interesting are the metallic hydrides of intermetallic compounds, in the simplest case the ternary system AB_xH_n, because the variation of the elements allows one to tailor the properties of the hydrides, see Table (1.1).

Table 1.1 The most important families of hydride-forming intermetallic compounds including the prototype and the structure. A is an element with a high affinity to hydrogen and B is an element with a low affinity to hydrogen.

Intermetallic compound	Prototype	Hydrides
AB ₅	LaNi ₅	LaNiH ₆
AB ₂	ZrV ₂	ZrV ₂ H _{5.5}
AB ₃	CeNi ₃	CeNi ₃ H ₄
A ₂ B ₇	Th ₂ Fe ₇	Th ₂ Fe ₇ H ₃
A ₆ B ₂₃	Y ₆ Fe ₂₃	Ho ₆ Fe ₂₃ H
AB	FeTi	FeTiH ₂
A ₂ B	NiMg ₂	Mg ₂ NiH ₄

Pant and Gupta [10] present following properties for the metal hydride to be an optimum hydrogen storage material:

1. High hydrogen capacity per unit mass and unit volume
2. Low dissociation temperature
3. Moderate dissociation pressure
4. Low heat of formation to minimize the energy necessary for hydrogen release and low heat dissipation during the exothermic hydride formation

5. Reversibility for limited energy loss during charge and discharge of hydrogen
6. Fast kinetics
7. High stability against moisture for a long cycle life
8. Cycleability
9. Low cost of recycling and charging infrastructures
10. High safety

The reaction of hydrogen gas with a metal is called the absorption process and can be described in terms of a simplified one-dimensional potential energy curve, see Fig. (1.2).

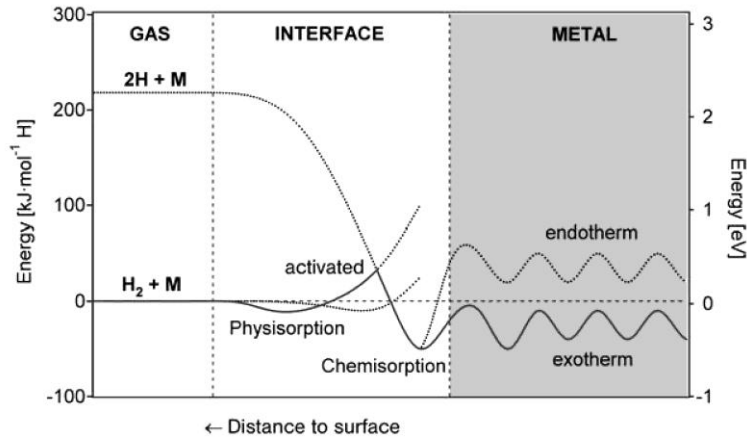


Figure 1.2 Lennard-Jones potential of hydrogen approaching a metallic surface [2].

Far from the metal surface the potentials of a hydrogen molecule and of two hydrogen atoms are separated by the dissociation energy. The first attractive interaction of the hydrogen molecule approaching the metal surface is the Van der Waals force, leading to the physisorbed state approximately one hydrogen molecule radius from the metal surface. Closer to the surface the hydrogen has to overcome an activation barrier for dissociation and formation of the hydrogen metal bond. The height of the activation barrier depends on the surface elements involved. Hydrogen atoms sharing their electron with the metal atoms at the surface are then at the chemisorbed state. The chemisorbed hydrogen atoms may have a high surface mobility, interact with each other and form surface phases at sufficiently high coverage. In the next step, the chemisorbed hydrogen atom can jump on the sub surface layer and finally diffuse on the interstitial sites through the host metal lattice [2].

The thermodynamic aspects of hydride formation from gaseous hydrogen are described by means of pressure-composition isotherms (PSI), Fig. (1.3). While the solid solution and hydride phase coexist, the PCIs show a flat plateau, the length of which determines the amount of stored H in the pure β -phase, the pressure rises steeply with the concentration. The two-phase region ends in a critical point, above which the transition from the α - to the β - phase is continuous [2].

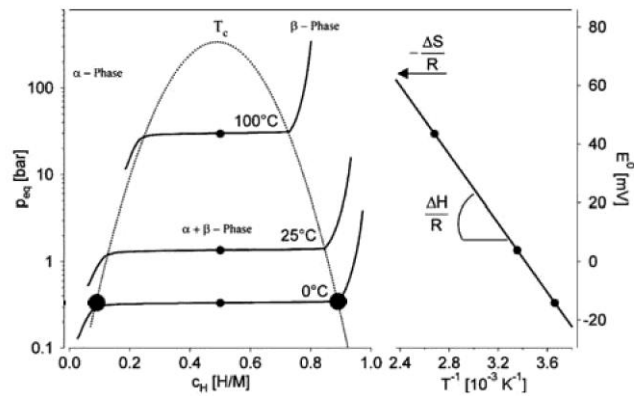


Figure 1.3 Pressure composition isotherms for hydrogen absorption in a typical intermetallic compound on the left hand side. The solid solution (α -phase), the hydride phase (β -phase) and the region of the coexistence of the two phases. The coexistence region is characterized by the flat plateau and ends at the critical temperature. The corresponding van't-Hoff diagram of the hydride is shown on the right side. When the change in heat capacity of materials involved in reaction is temperature independent, the van't-Hoff curves will be linear with the slope equal to $\frac{\Delta H}{R}$ [2].

An important feature in hydrogen storage by metal hydrides is the pressure plateau, which is a pressure at which the material reversibly absorbs/desorbs large quantities of hydrogen. For many applications, the pressure plateau should be close to ambient pressure, which allows the use of lightweight storage containers. Such pressure-concentration isotherms (PCI) are generally utilized for assessing the ability of metal hydrides to reversibly store hydrogen. PCI diagrams indicate the maximum attainable storage capacity and thermodynamic conditions for the reversible reaction. The pressure plateau can be tailored to a specific application through alloying. The equilibrium pressure depends strongly on temperature and is related to the changes in enthalpy and entropy. The entropy change corresponds mostly to the change from molecular hydrogen gas to dissolved hydrogen. At a given temperature, the pressure plateau represents one point on a pressure-

temperature (van't-Hoff) plot, Fig. (1.4) , where the log of pressure versus reciprocal temperature is linear with a negative slope. The slope related to the heat of reaction, that is, heat of hydrogenation [10].

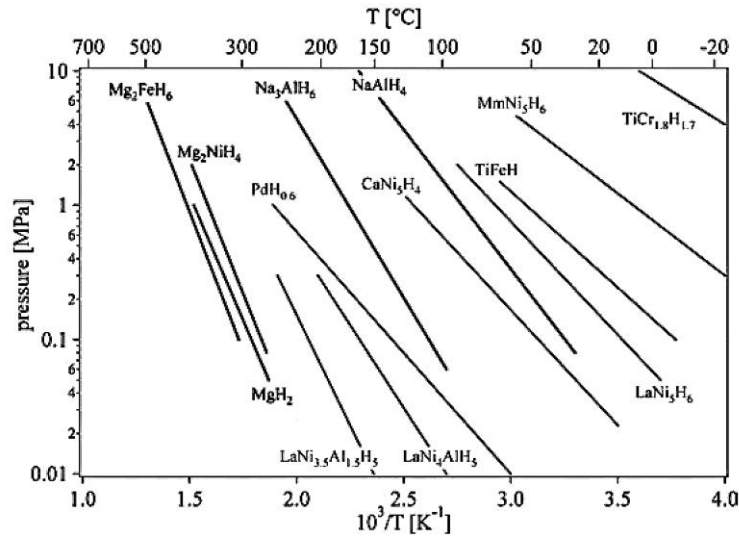


Figure 1.4 van't-Hoff plots for different metal hydrides [2].

Kinetics refers to the rates of hydrogen absorption and desorption. A faster kinetics at near ambient temperatures and pressures corresponds to less time at the fueling station while operating under safe conditions. Reaction kinetics of light metal hydrides depends on the surface area of the material exposed to hydrogen, the dimensions and homogeneity of the microstructure and the types of additives and catalysts.

Grant [12] mentions magnesium hydrides with the hydrogen capacity of 7.7 wt% and main drawbacks such as storing temperature, kinetics and susceptibility to contamination. The high heat of formation of magnesium hydride provides a major drawback to using the material as a hydrogen storage material owing to the high operating temperatures required. One approach is to reduce the heat of formation destabilizing the system by using additives that form compounds and alloys in either or both the hydrogenated or dehydrogenated states. However, another major problem is the slow hydriding and dehydriding kinetics. The absorption mechanism of MgH_2 at 600 K is said to initiate through the hydride forming at the magnesium grain surface and that its rate of formation is controlled by the density of nucleation sites.

Jensen, Wang and Chou [13] have worked on alanates as hydrogen storage materials. They are group I and II salts of $(AlH_4)^-$ and are currently referred to as complex hydrides. These materials have high hydrogen gravimetric densities and are, in most cases,

commercially available. The thermodynamics of the direct, reversible dehydrogenation of some complex hydrides lies within the limits that are required for a practical, on-board hydrogen carrier. All of these materials are, however, plagued by high kinetic barriers to dehydrogenation and/or rehydrogenation in the solid state. Despite the mentioned problems, Ti-doped sodium alanate to date stands as the hydrogen storage material with the best combination of material properties suited for vehicular hydrogen storage. However, its cycling hydrogen capacity is only 3-4 wt%.

Nakamori and Orimo [14] study borohydrides $M(\text{BH}_4)_n$ as hydrogen storage materials. They belong to a class of materials with the highest gravimetric hydrogen densities. Thermodynamic stability for $M(\text{BH}_4)_n$ can be systematically predicted by considering the electronegativity of metal M. Based on the correlation, one can expect that borohydrides with appropriate stability and high hydrogen density.

Gregory [15] expresses some work about imides and amides as hydrogen storage materials and mention them as a revolutionary new system of chemical hydrides that was neither based solely around metals and alloys nor depended on high surface area non-metals for the physisorption of hydrogen. In fact, the system was composed of both metallic and non-metallic elements in chemically distinct phases that were interconvertible by the making and breaking of non metal-hydrogen bonds. Lithium imide (Li_2NH) and lithium amide (LiNH_2) are well known hydrides in hydrogen storage career.

1.3 First principles studies

The last twenty years have seen a large deal of progress in the development of methods for ab initio calculations of materials properties and for simulations of processes in materials. Density Functional Theory (DFT) has the basic role for this development. The main idea of this theory is to cast the intractable complexity of the electron-electron interactions in many-electron systems into an effective one-electron potential, which is a functional of the electron density only [16].

DFT provides a general framework to deal with the ground state energy of the electrons in many atom systems. Today DFT is the method of choice for first principles electronic structure calculations in condensed phase and complex molecular environments. DFT based approaches are used in a variety of applications ranging from condensed matter physics, to chemistry, materials science, biochemistry and biophysics. Some reasons for this success are: (1) DFT converts the many-body electronic problem to a self-consistent-field single particle calculations. (2) despite the severe approximations made to the exchange and correlation energy functional, DFT calculations are usually accurate to

predict materials structures or chemical reactions products. (3) currently available computational power and modern numerical algorithms make DFT calculations feasible for realistic models of systems [17].

Many of the difficulties associated with the computational molecular structure have been overcome by more sophisticated theories that not only calculate the shapes and energies of molecular orbitals, but also predict by reasonable accuracy the structures and reactivity of molecules. The full treatment of molecular electronic structure is quite easy to formulate but difficult to implement [18].

In the Hartree-Fock equations the starting point is to write down the many electron wavefunction as a product of the one-electron wavefunction. There are two main strategies for continuing the calculations from this point. In the semi-empirical methods, many of the integrals are estimated by appealing to spectroscopic data or physical properties such as ionization energies and using a series of rules to set certain integrals equal to zero. In the ab initio methods, an attempt is made to calculate all the integrals that appear in the secular determinant. Both procedures employ a great deal of computational effort [18].

DFT has gained considerable ground in recent years to become one of the most widely used techniques for the calculation of molecular structure. Its advantages include less demanding computational effort, less computer time and better agreement with the experimental values than is obtained from Hartree-Fock procedures. The central focus of DFT is the electron density, rather than wavefunction. The energy of the molecule is a function of the electron density and the electron density is itself a function of position [18].

As in many other scientific and engineering subjects, first principles studies assisted extensively in understanding of hydrides, surface science and adsorption phenomena, electronic structure and charge transfer. Many properties of hydrides from hydrogen diffusion to electronic and band structure along with the energy for hydride formation have been studied with ab initio methods. Few studies are summarized in the following sections.

1.3.1 Ab initio studies on hydrides

Yang et al [19] used the linear-combination-of-atomic-orbit (LCAO) method for a cluster model in order to study the alloying effect on chemical bonding in TiH₂ type systems. They have calculated the electronic structures in pure dihydrides, such as ScH₂, TiH₂, VH₂, ZrH₂, and NbH₂ to verify that the cluster model is suitable. They have found that the alloying effect on the ionic interaction of alloyed TiH₂ is weaker than that on the covalent interaction and hydrogen makes a stronger covalent bond with the weaker hydride

forming elements and hydride non-forming elements rather than the stronger hydride forming elements if there is Ti atoms in the neighborhood in the alloyed TiH_2 . They have concluded that transition metal elements M would form weaker covalent bond with hydrogen atom in Ti(M)H_2 if M forms a more stable hydride MH_2 than TiH_2 .

Nishimia et al [20] have examined hydriding characteristics of zirconium-substituted FeTi. They discovered that zirconium substitution for titanium in FeTi made the activation treatments needless, lowered the equilibrium pressure in the β phase and narrowed the width of the plateau. The hydrogen capacity increases, but the reversible amount of hydrogen of practical importance decreases with the zirconium content owing to the increased residual amount of hydrogen. They believe a new ternary phase Fe_2TiZr would substantially be present and hydrogen atoms occupy the interstitial sites to form a solid solution $\text{Fe}_2\text{TiZrH}_4$.

Song et al [21] investigated the influence of titanium on the hydrogen storage characteristics of magnesium hydride. The results show a higher heat of formation of $\text{MgH}_2\text{-Ti}$ compared with that of MgH_2 . Besides, analysis of the density of states and charge distribution shows that the bonding between magnesium and hydrogen is weak, while the interaction between titanium and hydrogen is stronger. The results suggest that the hydriding/dehydriding kinetics of magnesium hydride can be improved by introducing titanium into the compound.

C. Wolverton et al [22] present an overview of their recent efforts aimed at developing a first-principles computational approach for the discovery of novel hydrogen storage materials. They present examples that illustrate each of the following capabilities: (1) prediction of hydriding enthalpies and free energies across a wide range of hydride materials, (2) prediction of low energy crystal structures for complex hydrides, and (3) predicted decomposition pathways for metal hydrides. The electronic-structure total energy calculations in this study are based on density-functional theory (DFT), as implemented in the highly efficient VASP code.

A. Kinaci and K. Aydinol in their study [23] have found that, the insertion of hydrogen into the structure causes an increased electron density in the electronic orbitals of Fe which were oriented towards hydrogen atoms. They have also identified a new hydride which is less stable than the experimentally observed ones, having four hydrogen atoms per chemical formula. In this study, first principles pseudopotential calculations of FeTiH_x ($x = 1-6$) hydrides are presented. The calculations mainly focused on the subgroups of $Pm\bar{3}m$ space group, in which Fe-Ti coordination is similar to the one in $Pm\bar{3}m$. In addition, experimental structures were also considered. As a conclusion, they have reached to the

solution that ab initio results are in agreement with experimentally determined ground states for FeTiH and FeTiH₂. Also the formability of a higher H content structure, FeTiH₄, have been predicted in this research. Although it seems unstable, it is nearly stable or can be made stable with some chemical makeup. It is also found that storing more H above H/M=2 into FeTi chemistry seems to be unlikely. The primary octahedral framework of FeTiH is conserved when it is transformed into FeTiH₂ and hydrogen additions produce a second kind of octahedral site. However, this octahedral metal organization around H has changed to tetrahedral framework for FeTiH₄, causing an increase in formation energy of this compound.

1.3.2 Ab initio studies on adsorption

The adsorption of a gas on a surface is a consequence of the field force at the surface of the solid, called the adsorbent, which attracts the molecules of the gas or vapor, called adsorbate. The origin of the physisorption of gas molecules on the surface of a solid are resonant fluctuations of the charge distributions and are therefore called dispersive interactions or the Van der Waals interactions. In the physisorption process, a gas molecule interacts with several atoms at the surface of the solid. The interaction is composed of two terms: an attractive and a repulsive term which diminish with the distance with the molecule and the surface. Therefore, the potential energy of the molecule shows a minimum at a particular distance. Once a monolayer of the adsorbate molecules is formed, the gaseous molecules interact with the adsorbent surface [24].

Lee et al [25] have investigated the adsorption of hydrogen on FeTi surfaces via ab initio methods. They have discussed the driving bonding mechanisms for different adsorption sites in (001) and (110) surfaces. They have found that the hydrogen atoms form stronger chemical bonds with the iron atoms compared to the titanium atoms. They have also studied the local density of states (LDOS) of surfaces and the contour plots of the charge density distribution in the plane perpendicular to surfaces. As a result, they indicate the interactions between hydrogen and FeTi surface are strongly influenced by the position of the adsorbed hydrogen. they mentioned increasing of the density of states at the Fermi level during hydrogen charging in all the cases. This causes a weakening of interatomic bonds and phase instability.

Yakovin [26] studied oxygen adsorption on W(112) surface within DFT simulations. He has found quasi three fold hollow sites favored for oxygen adsorption for a monolayer coverage and the bridge-on-row sites for a half monolayer coverage. He has also studied the stability of the W(112) surface under oxygen adsorption and the surface

relaxation which is accompanied by the redistribution of density of states, associated with transformations of surface states. He described the changes in surface electronic structure induced by oxygen adsorption as the shift of surface states towards higher electron binding energies.

Jiang et al [27] worked on adsorption and dissociation of CO on Fe(110) surface from first principles. They employed spin-polarized periodic density functional theory and investigated the site preference of CO adsorption for two different coverages. They have also calculated heats of adsorption, CO stretching frequencies and work function changes. For the next step, they have studied dissociation from the on-top site using the Climbing Image Nudged Elastic Band method (CI-NEB) to a lying-down transition state, from the on-top site to the long-bridge site and from the long-bridge site to the on-top site. They have found a high barrier (1.52 eV from the on top site) for CO dissociation on Fe(110) and related that to the decomposition of CO on Fe(110) which only occurs at high temperatures. They also mentioned that the CO dissociation is competitive with molecular desorption and after dissociation, O atoms remain on the surface while C atoms diffuse into Fe(110), presumably as the initial step towards carburization of Fe.

Chen et al [28] studied the mechanism of adsorption and dissociation of water molecule on W(111) surface at the DFT level. They have shown that the most favorable structure of W(111) – H₂O corresponds to the coordination of water through its oxygen lone pairs with the W(111) surface at its top position. The preferable binding sites for the OH, O, and H fragments are top, top and bridge sites, respectively. They have constructed a potential energy surface for the decomposition of water on W(111) and found the barriers of H₂O dehydrogenation equal to 1.8 kcal/mol for the H-OH bond activation and 15.9 kcal/mol for the O-H bond activation.

Banerjee et. al [29], using first principle calculations, have investigated the interaction of hydrogen molecules with both clean and metal doped Mg(0001) surfaces. They have found that on the basis of the energetic criteria, studied atoms of Ti, V and Ni prefer to substitute one of the Mg atoms from the second layer rather than the top surface atom. The results of the interaction of a hydrogen molecule with the clean and doped Mg surface, shows that for metal atoms at the surface, the hydrogen molecule undergoes spontaneous dissociative chemisorptions. However, for metal atoms in the second layer, it requires to cross an activation barrier to undergo molecular dissociation. Regarding stability criteria, the substitutional energies of studied doping elements have been found to be negative and they prefer to substitute one of the Mg atoms from the second layer rather than that from the top surface layer.

Busnengo and Martinez [30] worked on H₂ chemisorption on W(100) and W(110) surfaces. They have obtained properties of the clean surfaces and have built accurate six-dimensional potential energy surfaces (PESs) used to compute dissociative sticking probabilities of on both faces of W through classical trajectory calculations. Their calculations have shown that dissociative adsorption of H₂ on both W(100) and W(110) is a non-activated process.

D. Kecik and K. Aydinol in their paper [31] tried to propose new Mg alloys with improved desorption characteristics where the context of the study basically comprises: calculation of formation energies of alloyed bulk MgH₂ structures and alloyed Mg surface structures by total energy pseudopotential methods and investigation of the effect of substitutionally adsorbed dopants to the desorption behavior of hydrogen molecule at the surface via ab initio Molecular Dynamics (MD). In these bulk and surface alloying studies thirty two and in MD studies thirteen alloying elements were considered. According to their results, 31 out of 32 dopants seem to have decreased the formation energy (in absolute manner) of bulk MgH₂, within a range of nearly 42 kJ per one mole of hydrogen. On the other hand, Results point out that elements such as Mo, Nb, Mn, Cr, Co, Fe, V, P and Ni help the dissociation of hydrogen molecule on the surface.

In this study, surface characteristics of Iron-Titanium alloys have been studied in both pure and alloyed forms and hydrogen adsorption behavior of pure surfaces was determined via ab initio pseudopotential-planewave method within the projector augmented wave (PAW) scheme to density functional theory (DFT). PBE functional form of the generalized gradient approximation (GGA) has been chosen to electron exchange and correlation within DFT.

CHAPTER 2

METHODOLOGY

In this study, all calculations were performed in a plane wave basis set using the projector augmented wave (PAW) method [32] within the formalism of density functional theory as implemented in the VASP program [33-35]. In the calculations, PAW potentials [36] were used, where exchange-correlation functional with the generalized gradient approximation (GGA) is in PBE form [37].

Initially, bulk calculations in FeTi, FeTiH and FeTiH₂ structures were performed for several test purposes. Following bulk calculations, simulation cells having free surfaces of three different crystallographic planes; (001), (110) and (111) in the FeTi structure were set up. Considering the constituent elements Fe and Ti, (001) and (111) can have two different terminations. Therefore a total of five different surface structures were studied. Initially, the unalloyed surface structures were calculated. Over these surfaces, H₂ and H adsorption sites were determined and probable dissociation paths for the H₂ molecule were postulated by the analysis of the calculated adsorption energies. Then selected elements from the 3-D transition metals were substituted with one surface atom (Fe and Ti separately). After calculations, surface relaxation and reconstruction due to alloying and the adsorption energies of the substituent elements were determined.

2.1 Bulk calculations

FeTi adopts the CsCl structure (B2 – Strukturbericht notation) which has the symmetry of the $Pm\bar{3}m$ (221) space group. Hydrides of this intermetallic; however, adopt an orthorhombic crystal structure. The crystal structure details are given in Table (2.1). After setting up the simulation cells in the bulk sense with periodic boundary conditions, the cell volume and the atomic positions are allowed to relax to find the minimum energy configuration. During these calculations, sampling in the reciprocal space (k -point grid size) and spin polarization effect were considered to attain a few meV convergency. For FeTi, FeTiH and FeTiH₂ structures, it was found that 24×24×24, 20×20×20 and 16×16×24

Gamma centered grid of k-point sampling was adequate, respectively. Expectedly, since Fe is a magnetic element, the total energies of the compounds changes with respect to spin polarization. However, in the calculated formation energies the difference was found to be less than 50 meV. Therefore, spin polarization was not considered in further calculations. The formation energies of the hydrides were calculated considering the below generic hydrogenation reaction:



as;

$$\Delta E_f = \frac{2}{n} E_{FeTiH_n} - \frac{2}{n} E_{FeTi} - E_{H_2} \quad (2.2)$$

The coefficients of the reaction were normalized to define the formation energy per one mole of H₂ gas, so as to simplify comparison. The energy of H₂ is approximated to the energy of an H₂ molecule in vacuum at zero Kelvin, thus entropy term is neglected. The calculated crystal structure parameters and formation energies of the compounds are given in Table (2.1), comparatively with the available experimental data. As can be seen, the disagreement between the calculated and the experimental lattice parameters is at maximum 2.6%, which is quite acceptable in ab initio calculations. The agreement in the formation energy of the compounds is fairly good, where the discrepancy is approximately 10-15 %.

Table 2.1 Calculated crystal structure parameters and formation energies of the hydrides. Experimental data is given in parenthesis. Crystal structure data for FeTi, FeTiH and FeTiH₂ are due to [38], [39] and [40] respectively. Experimental formation energy data are from [41].

Compound	Space Group	Wyckoff Positions			Structure Parameters (Å)			Formation Energy kJ/mole of H ₂
		Fe	Ti	H	a	b	c	
FeTi	221	1a	1b	-	2.945 (2.9789)	-	-	-
FeTiH	17	2c	2d	2a	2.889 (2.956)	4.529 (4.543)	4.264 (4.388)	25.28 (28.1)
FeTiH ₂	65	4i	4h	2a+2c+4e	6.957 (7.029)	6.071 (6.233)	2.769 (2.835)	26.86 (31-33.7)

2.2 Surface calculations

2.2.1 Pure surfaces

Three different crystallographic surfaces, (001), (110) and (111) were considered for hydrogen adsorption. Slabs of FeTi, see Fig. (2.1), consisting of a 3x3 surface unit cell, were created with 8, 7 and 12 atomic layers for (001), (110) and (111) surfaces, respectively. The position of atoms in the surface structures was set according to the relaxed coordinates in bulk FeTi. In the cells, a 15 Å thick vacuum layer was put along the z-direction so as to mimic the free surface. The cell volume and the two very bottom atomic layers were fixed during the calculations to impose the bulk condition as going down below the surface; however, the rest of the top lying atoms were allowed to relax fully until 1 meV convergence is obtained in the total energy. In all surface calculations, a Gamma centered grid of 3x3x3 *k*-point set was used corresponding to 6 *k* points in the irreducible Brillouin zone, together with a first order Methfessel-Paxton [42] smearing of width $\sigma=0.2$ eV. In the expansion of the plane-wave basis set, a kinetic energy cutoff of 280 eV was used. Overall the convergence in the total energy is less than 1 meV per unit cell.

2.2.1.1 Molecular and atomic hydrogen adsorption

One of the major concerns in hydrogen storage in solid hydrides is the ease of hydrogen intake reaction taking place at the particle surface. Even if there may be a strong thermodynamic affinity for this reaction, many times it is limited by kinetic reasons[43,44]. The major kinetic barrier is at the dissociation stage of the H₂ molecule over the surface [45-47]. Therefore, in practical applications catalysts are used [47,48]. For this reason understanding of the surface states and adsorption sites for H₂ molecules and dissociated H atoms is crucial.

In this study for all surfaces under investigation, considering all possible adsorption sites, H and H₂ adsorption energies were determined in order to identify the most probable dissociation path of the H₂ molecule. The details of calculations are identical with the pure surface calculations. In both Fe and Ti terminated (001) surfaces, the high symmetry adsorption sites are top, bridge and four-fold hollow positions, see Fig. (2.2). In (111) surface similarly, there are top, bridge, three-fold FCC hollow and three-fold HCP hollow sites as can be seen from Fig. (2.3). The number of high symmetry sites are numerous in (110) surface, see Fig. (2.4). They are Fe-top, Ti-top, Fe-Fe bridge, Ti-Ti bridge, Fe-Ti bridge.

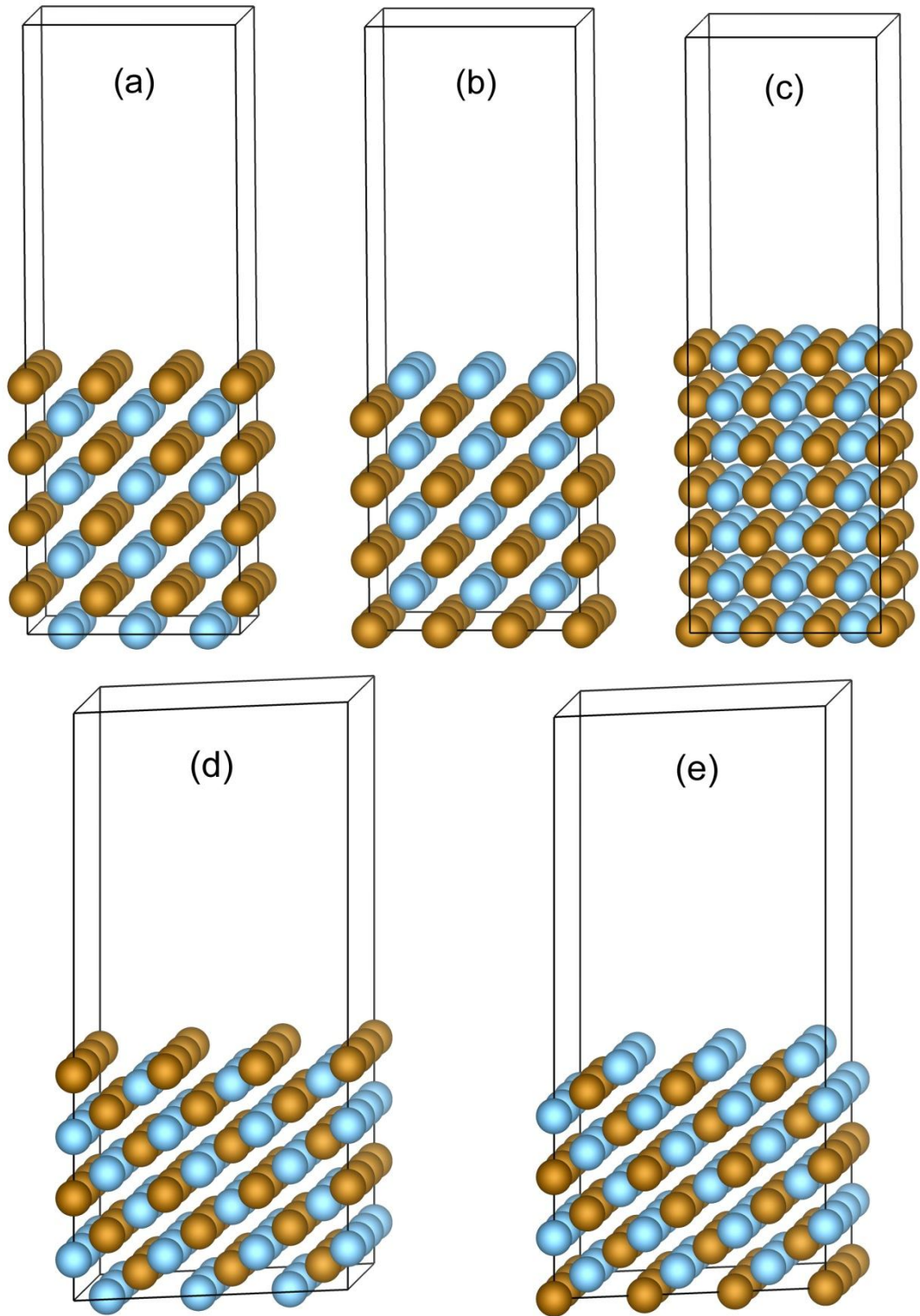


Figure 2.1 Simulation cells for the surface studies. (a) Fe-terminated (001) surface, (b) Ti-terminated (001) surface, (c) (110) surface, (d) Fe-terminated (111) surface and (e) Ti-terminated (111) surface. Brown and blue spheres represent Fe and Ti atoms, respectively.

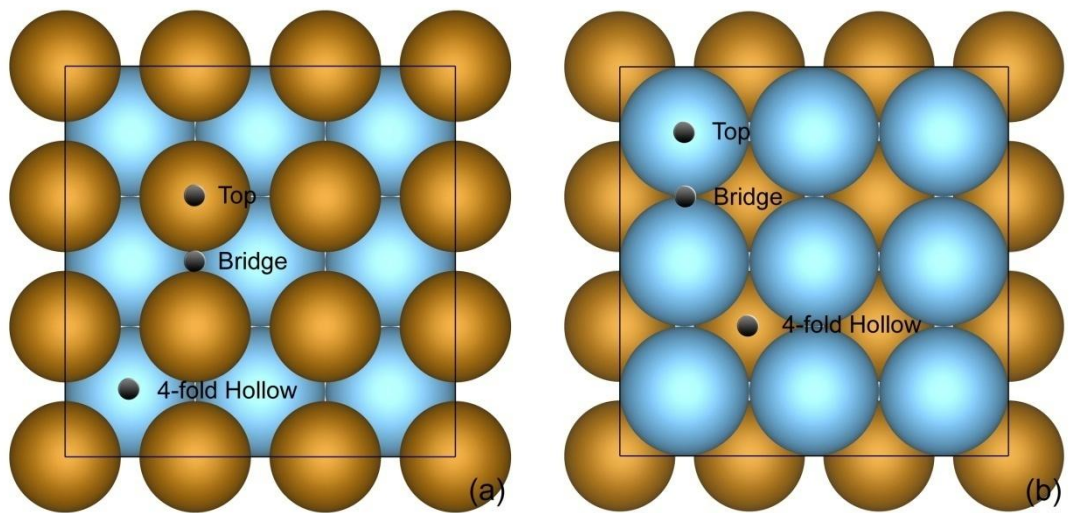


Figure 2.2 High symmetry sites for adsorption on (a) Fe and (b) Ti terminated (001) surfaces. Brown and blue spheres represent Fe and Ti atoms respectively.

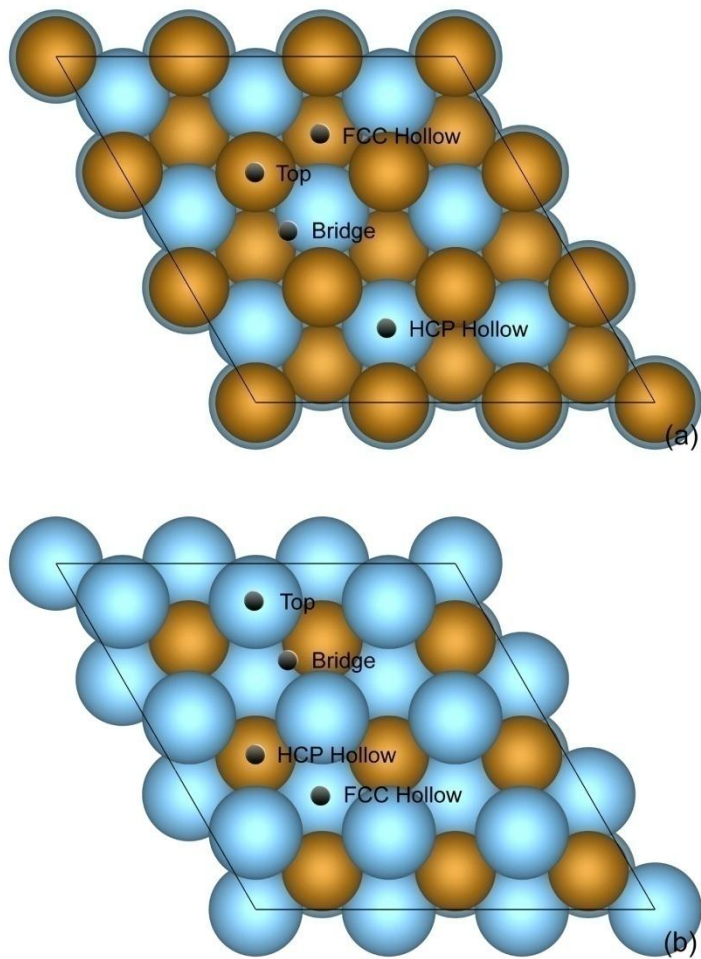


Figure 2.3 High symmetry sites for adsorption on (a) Fe and (b) Ti terminated (111) surfaces. Brown and blue spheres represent Fe and Ti atoms respectively.

There are four three-fold sites more, which are (Ti-Ti)_L-Fe, (Ti-Ti)_S-Fe, (Fe-Fe)_L-Ti and (Fe-Fe)_S-Ti. H₂, since it is a linear molecule, can be positioned at these high symmetry sites in different ways. Namely, vertical in which the H-H axis is perpendicular and horizontal where the H-H axis is parallel to the surface plane. Apart from this, in horizontal configuration of the H₂ molecule, there is one more degree of freedom which considers the alignment of the H-H linear axis over the surface. Different alignments over all studied surfaces were labeled accordingly as given in Fig. (2.5). Afterwards, an atom of H and vertically and horizontally aligned molecule of H₂ (having two hydrogen atoms separated by equilibrium distance, calculated to be 0.7548 Å) were put on these sites at 1.5 Å above the surface plane. They are then (including the previously allowed surface layers) relaxed to obtain the minimum energy configuration. In order to avoid the motion of the atom or the molecule from the initial site to a more favorable nearby position, so that a physisorbed atom's or molecule's adsorption energy specific to the initial site is obtained, the hydrogen molecule or atom is not allowed to relax in the x-y plane. Adsorption energy then can be calculated considering the following adsorption reaction:

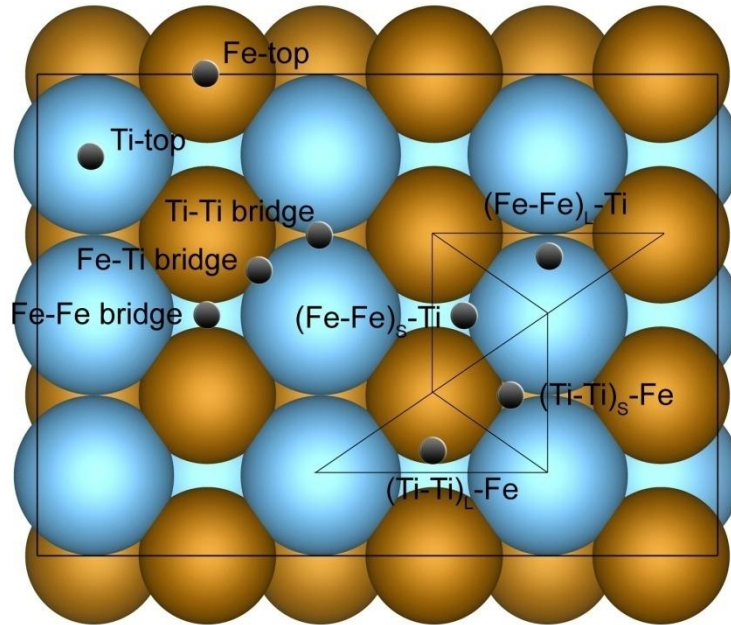
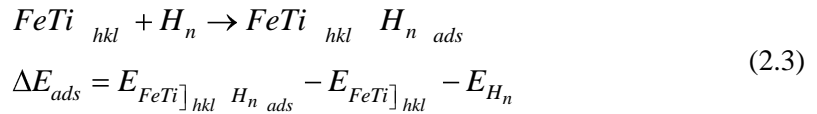


Figure 2.4 High symmetry sites for adsorption on (110) surface. In case of three-fold hollow sites, the related triangles are shown with solid black lines. Brown and blue spheres represent Fe and Ti atoms, respectively.

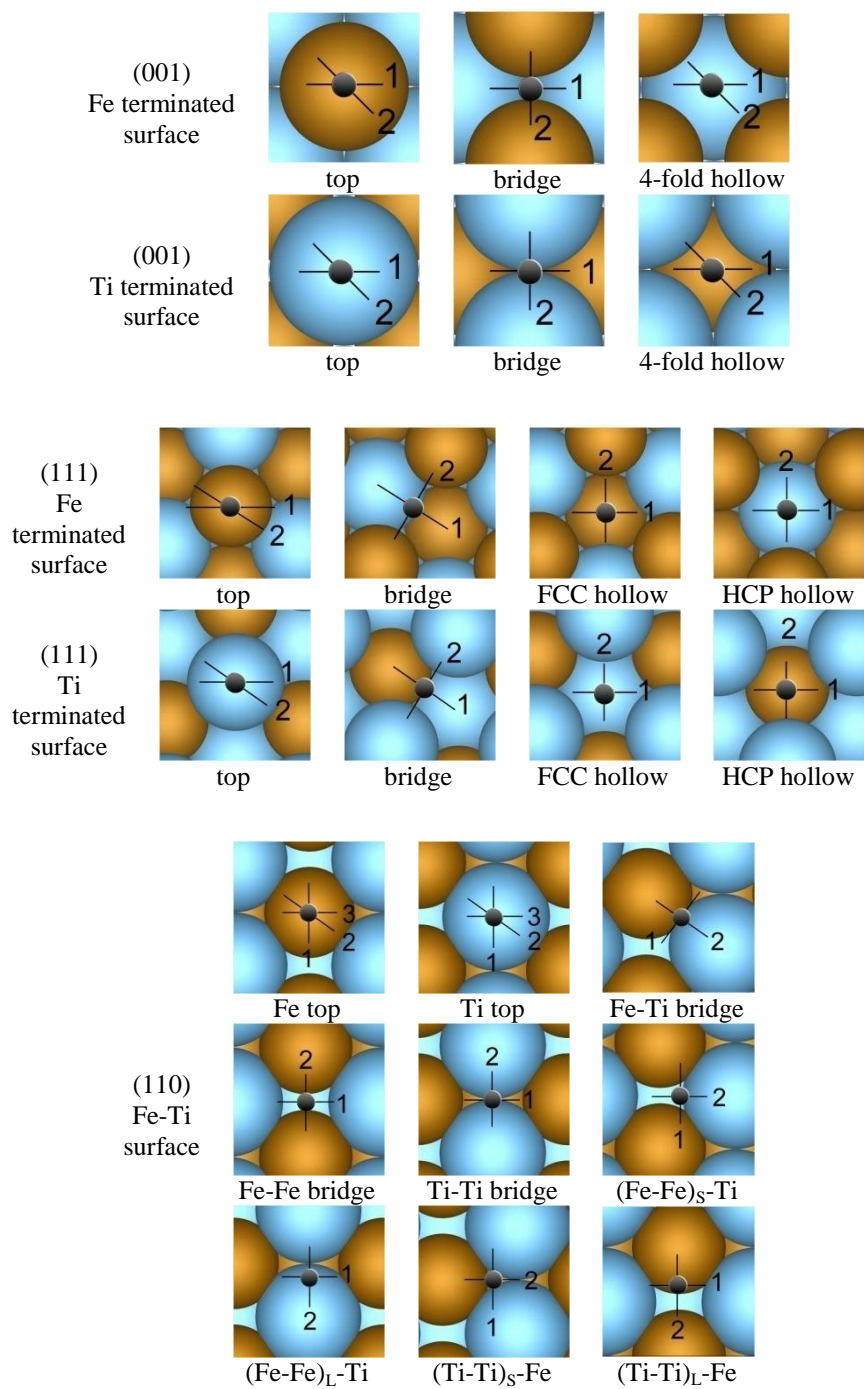


Figure 2.5 Labeling of the alignment of H₂ molecule where its linear axis is set horizontal to the surface.

The nudged elastic band (NEB) method, widely used for locating transition states, is an efficient method for finding the minimum energy path (MEP) between a given initial and final state of a reaction [49-51]. An initial path is constructed and represented by a discrete set of images of the system connecting the initial and final states. Adjacent images are connected by springs, mimicking by elastic band and the tangent of the path is estimated on each image. An optimization of the band, mainly the minimization of the forces acting on images, brings the band to the MEP.

The MEP can be used to estimate the activation energy barrier for transitions between the initial and final states. Any maximum along the MEP is a saddle point on the potential surface and the energy of the highest saddle point gives the activation energy of the reaction. It is important to ensure that the highest saddle point is found. It is quite common to have MEPs with one or more intermediate minima and the saddle point closest to the initial state may not be the highest saddle point for the transition [49].

The climbing image NEB (CI-NEB) method constitutes a small modification of the NEB method [50]. Information about the shape of the MEP is retained, but a rigorous convergence to a saddle point is obtained. With the climbing image scheme, the highest energy image climbs uphill to the saddle point. This image does not feel the spring forces along the band, but the true force at this image along the tangent is inverted. In this way, the image tries to maximize its energy along the band and minimize it in all other directions. When this image converges, it will be at the exact saddle point [50].

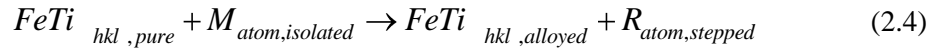
In this study, we used CI-NEB method to calculate the MEP for the dissociation of hydrogen molecule over several FeTi surfaces and to determine the activation energy of the process. In the calculations; however, a smaller k -point grid, 3x3x1 is employed to reduce computational cost.

2.2.2 Alloyed surfaces

We next aimed to investigate the substitutional adsorption behavior of 3d transition metals (from Sc to Zn) on the selected surface structures of FeTi. The same simulation cells, as given in Fig. (2.1) and computational parameters were used for the alloying study. For each of five different surface structures, the alloying atom, M is substituted in place of either Fe or Ti atom at the very top layer. However in (110) surface, since both Fe and Ti reside on same layer, they are substituted separately. For the purpose of obtaining the lowest energy configuration, systems were allowed to relax in terms of all atomic degrees of freedom, while the cell size and shape were kept constant. The dipole corrections to the total energy was also considered for the alloyed surfaces, which was found to be less than 1

meV per cell. Due to alloying, the plane symmetry in the surface is changed, thus the symmetry constraint in VASP program can lead to erroneous surface structure during relaxation. For this purpose, the symmetry constraint was switched off and compared with symmetry on calculations for several different surfaces with several different alloying additions. The results showed a negligible difference in terms of both energy and atomic positions, therefore for further calculations dipole corrections and non-symmetric calculations were not taken into account.

The substitutional adsorption reaction occurring on a surface has the following steps. Initially a host atom at the surface must leave its position forming a surface vacancy behind, where it should later form a step or kink somewhere else on the surface. Then an alloying element that comes from an infinite distance occupies that vacant position. The overall adsorption reaction for FeTi then can be written as such,



where M is the alloying element and R is the replaced element (Fe or Ti). The adsorption energy for a substitutionally doped FeTi surface is then calculated from the below equation.

$$\Delta E_{ads-subst} = \left(E_{FeTi}_{hkl,alloyed} + E_{R_{atom,stepped}} \right) - \left(E_{FeTi}_{hkl,pure} + E_{M_{atom,isolated}} \right) \quad (2.5)$$

Therefore, two different energy terms should further be calculated. The first one is the isolated alloying element energy and the other one is the energy for step formation on each surface studied, both for Fe and Ti atoms.

Energies for isolated atoms can be calculated by putting the alloying element in a very large box. However, specific to atoms and molecules several points should further be considered. In the calculation of the isolated atom energies, Gamma-point only reciprocal space sampling is required since Bloch theorem does not apply in this case. In addition, in the handling of the partially occupied bands during wavefunction setting, Gaussian smearing with a small smearing width (less than 0.05 eV) should be preferred rather than usual Methfessel-Paxton scheme. Otherwise it may cause unphysical electronic entropy, which is a meaningless quantity for atoms and molecules.

Step formation energy is the energy required to form an adatom of the same kind, as if the surface extends towards vacuum by the transport of the atom to a step or kink site at the surface. In this respect, it can simply be evaluated as the difference of energies of a

cell having perfect surface geometry and the cell having this step. Therefore, the position of this step over the surface should be known. For (110) surface structure, this step site is simply the regular lattice position over the surface, since there are both Fe and Ti sites defined on this crystallographic plane. However, for (001) and (111) surfaces, the removed atom from the surface (Fe or Ti) cannot be put to an extended lattice position over it, since in the regular lattice definition, in the above layer the site should be occupied by the other type of atom (Ti or Fe). Therefore, for (001) and (111) surfaces, high symmetry step sites over them should be determined and the one that has the minimum in adsorption energy must be considered as the most stable step site for the respective surface structure. These high symmetry positions are top, bridge and hollow sites as usual. After calculations, the favorable step sites came out to be the four-fold hollow sites for (001) and FCC hollow sites for (111) surfaces in both terminations.

CHAPTER 3

RESULTS AND DISCUSSIONS

3.1 Pure surfaces

3.1.1 Surface structure, relaxation and reconstruction

Quantifying the structure of surfaces and particularly of adsorbates on surfaces, relaxation is a key step to understand many aspects of the behavior of surfaces including the electronic structure and the associated chemical properties. The outermost atomic layers of a solid generally have layer spacing which differs from that of the underlying bulk as a consequence of the termination of the solid. Typically the outermost layer spacing is contracted, the second layer spacing expanded and so on, although the amplitude of this relaxation damps rapidly with depth.

The clean surface interlayer distance relaxations of clean surface from bulk values, are shown in Table (3.1) for all studied surfaces of FeTi.

Table 3.1 The clean surface interlayer distance relaxations of surfaces from bulk values.

Surface	Δd_{12}	Δd_{23}	Δd_{34}	Δd_{45}	Δd_{56}	Δd_{67}	Δd_{78}
(001) Fe terminated	-18.2	7.7	-6.5	4.4	-3.6	-	-
(001) Ti terminated	-7.9	4.9	-2.1	1.4	-2.6	-	-
(110) Fe-Fe spacing	-8.0	1.2	-0.8	-0.3	-	-	-
(110) Ti-Ti spacing	0.3	0.7	0.4	0.5	-	-	-
(111) Fe terminated	-30.2	-5.0	-3.1	4.6	-2.6	4.5	-1.3
(111) Ti terminated	1.7	-20.6	0.1	4.1	1.9	1.7	-2.4

Here, Δd_{nm} corresponds to the difference in the distance between n^{th} and m^{th} layer in bulk and relaxed calculations in percentage. Therefore, the negative values indicate contraction in layer spacing, while positive numbers show expansion with respect to the bulk layer separations. Here, $n=1$ represents the surface layer, $n=2$ relates to the sub-surface layer and so on.

Results obtained from (001) surfaces in both terminations, show a perfect order in relaxation values. The topmost layer spacing shows a contraction of about 18% for Fe-terminated and 8% for Ti-terminated surfaces. The next layer spacing shows an expansion for both terminations and this contraction-expansion cycle can be seen till the last relaxed layer. On the other hand, the absolute amount of change in layer spacing decreases as going down into the slab. Only the last interlayer distance in Ti-terminated (001) surface expresses an exception. Comparing layer spacing between identically numbered layers in Fe- and Ti-terminated (001) surface, it is clear that the amount of contraction and expansion is about two times bigger in Fe-terminated (001) surface compared to Ti-terminated one. As a result, in case of FeTi (001) surface, the Fe-terminated one shows more relaxation.

The (110) crystallographic plane is composed of both Fe and Ti atoms. During relaxation of the surface structure having (110) symmetry, it was recognized that Fe and Ti atoms in the same layer behave differently in a coordinated manner; which means, each layer dissociates into two Fe and Ti sub-layers. In all layers of this structure, Ti-Ti spacing show very little expansion, while the topmost Fe-layer spacing experiences considerable amount of contraction, therefore the top layer becomes Ti terminated. Nevertheless, the absolute amounts of these changes are smaller than that of (001) surface in both terminations.

Relaxation in the (111) surface is somewhat similar to the relaxation phenomena observed in other surfaces. Especially the outermost Fe-layer spacing, whether the top layer in Fe-terminated or the layer below the top in Ti-terminated (111) surfaces, show considerable contraction while Ti-layer spacing express less expansion.

It is also found that, the reconstruction (atomic rearrangements within the plane) in pure surfaces of FeTi does not occur, which is expected since the lateral order in FeTi surfaces is not destroyed by impurity atoms or vacancies.

3.1.2 Hydrogen adsorption energies

The adsorption energies of horizontal and vertical hydrogen molecule and hydrogen atom, for all labeled positions as given in Fig. (2.5) are shown in Table (3.2), which were calculated according to Eq. (2.3).

Between horizontal and vertical hydrogen molecule adsorption, it is clear that in almost all of the identical high symmetry adsorption sites, the adsorption energy of vertical molecules are higher than that of the horizontal alignment. Therefore as a result, H_2 is more likely to be adsorbed on all studied FeTi surfaces rather horizontally than vertically.

Here, two sites show exception. In Ti-terminated (001) surface, the 4-fold hollow site is a little more convenient for vertical molecule adsorption rather than the horizontal one. However, for this surface symmetry the lowest energy adsorption site is the top site (either [1:] or [2:] alignment) where H_2 lies horizontal. The other exception is on (110) surface, Fe-Fe bridge site where the adsorption energies of two horizontal molecules are positive which means this site cannot adsorb a horizontal molecule. The vertical molecule is therefore the least energy position for this site. But again it cannot be considered as an adsorption site for the hydrogen molecule compared to other low energy sites on this surface.

In case of atomic hydrogen adsorption on (001) surface, as it can be seen from Table (3.2) for both Fe- and Ti- terminated surfaces, the bridge site is the most favorable site. For hydrogen molecule; however, the top site is the most favorable for adsorption. A very small difference of the order of 1 meV exists between different alignments of hydrogen molecule on the top site of both Fe- and Ti-terminated (001) surface. In both situations the top [1:] site is slightly more favorable rather than top [2:] site. It suggests that on this surface the molecule alignment does not affect the adsorption of hydrogen molecule notably. Considering both favorable adsorption sites for atomic and molecular hydrogen, a clearly reasonable hydrogen molecule dissociation path on FeTi (001) surface can be revealed. In both terminations the hydrogen molecule is being adsorbed on the top site of surface atoms preferably along the position [1:] of Fe- and Ti- terminated top sites. After overcoming the probable activation energy for dissociation, the hydrogen atoms within the molecule begin to separate and the distance between them increases. Meanwhile the movement of the departing atoms would be along the initial molecule axis, where the separated atoms are directly brought to the favorable bridge sites for atomic hydrogen as depicted in Fig. (3.1).

Table 3.2 Calculated adsorption energies of H atom and H₂ molecule over all studied surfaces of FeTi.

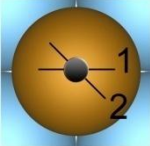
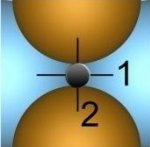
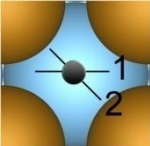
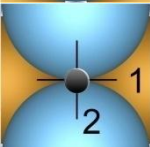
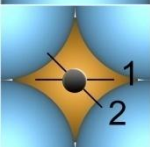
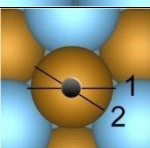
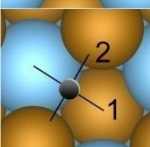
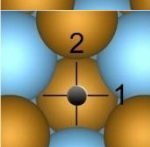
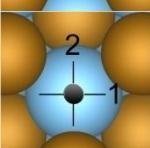
Adsorption Site		Adsorption Energy (eV)			
		H ₂ (horizontal)	H ₂ (vertical)	H	
(001) Fe terminated surface	Top		[1:] -0.463	-0.013	-2.128
			[2:] -0.462		
	Bridge		[1:] -0.074	0.008	-2.863
			[2:] -0.011		
	4-fold Hollow		[1:] -0.013	-0.010	-2.755
			[2:] -0.017		
(001) Ti terminated surface	Top		[1:] -0.917	-0.379	-2.832
			[2:] -0.913		
	Bridge		[1:] -0.842	-0.420	-3.526
			[2:] -0.391		
	4-fold Hollow		[1:] -0.412	-0.418	-3.434
			[2:] -0.409		
(111) Fe terminated surface	Top		[1:] -0.379	-0.035	-2.220
			[2:] -2.231		
	Bridge		[1:] -1.676	0.002	-4.504
			[2:] +0.056		
	FCC Hollow		[1:] -0.104	0.019	-4.498
			[2:] -0.104		
	HCP Hollow		[1:] -0.184	0.002	-2.540
			[2:] -0.183		

Table 3.2 Continued.

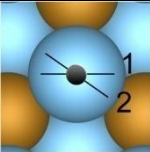
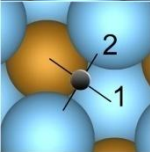
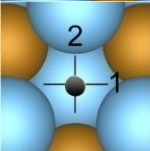
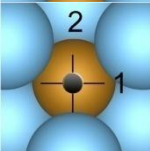
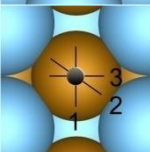
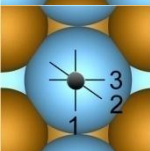
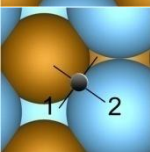
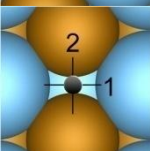
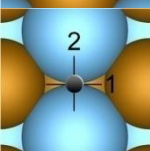
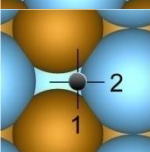
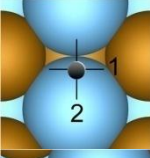
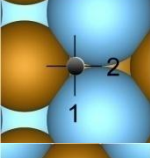
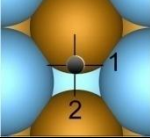
Adsorption Site		Adsorption Energy (eV)			
		H ₂ (horizontal)	H ₂ (vertical)	H	
(111) Ti terminated surface	Top		[1:] -0.151 [2:] -0.151	0.004	-1.853
	Bridge		[1:] -0.022 [2:] -	-0.001	-3.140
	FCC Hollow		[1:] 0.017 [2:] -0.008	-0.001	-2.414
	HCP Hollow		[1:] -0.006 [2:] -0.011	0.007	-3.032
(110) surface	Fe Top		[1:] -0.470 [2:] -0.527 [3:] -0.562	-0.019	-2.831
	Ti Top		[1:] -0.195 [2:] -0.176 [3:] -0.161	-0.007	-1.547
	Fe-Ti Bridge		[1:] -0.182 [2:] 0.015	0.023	-2.957
	Fe-Fe Bridge		[1:] 0.140 [2:] 0.095	-0.009	-3.124
	Ti-Ti Bridge		[1:] -0.137 [2:] -0.008	-0.007	-2.759
	3-fold (Fe-Fe) _s -Ti Hollow		[1:] -0.095 [2:] -0.048	-0.006	-2.510

Table 3.2 Continued.

Adsorption Site		Adsorption Energy (eV)			
		H ₂ (horizontal)	H ₂ (vertical)	H	
(110) surface	3-fold (Fe-Fe) _L -Ti Hollow		[1:] -0.081	0.028	-2.261
			[2:] -0.114		
	3-fold (Ti-Ti) _S -Fe Hollow		[1:] -0.055	0.172	-3.268
			[2:] -0.355		
	3-fold (Ti-Ti) _L -Fe Hollow		[1:] -0.384	0.125	-2.887
			[2:] -0.599		

The minimum energy path (MEP) for the dissociation of the hydrogen molecule over Fe and Ti terminated (001) surfaces were calculated using the CI-NEB method and the corresponding activation energies were determined, see Fig. (3.2). In CI-NEB calculations, initially four equally spaced images were constructed between the initial and final states. The initial and final states of the dissociation are assumed to be as given in Fig. (3.1). As can be seen, for the initial state, top [1:] site for H₂ molecule and for the final state, bridge site for the hydrogen atom are the most stable adsorption sites. Along the dissociation pathway, the H-H bond length starts to increase from its equilibrium value to finally 3.1 Å and 2.8 Å for Fe and Ti cases, respectively. Meanwhile, the bridge length in both cases initially decreases slightly and increases again upon further dissociation. The activation energy for the dissociative adsorption of hydrogen was determined to be 0.178 and 0.190 eV for Fe and Ti terminated (001) surfaces, respectively. Although these activation energies are not that high to limit the reaction rate considerably, from the adsorption rate measurements made in activated samples of FeTi powders [52]; however, it was concluded that the activation energy for adsorption is zero. This experimental observation, therefore indicates a more favorable dissociation path in another surface of FeTi.

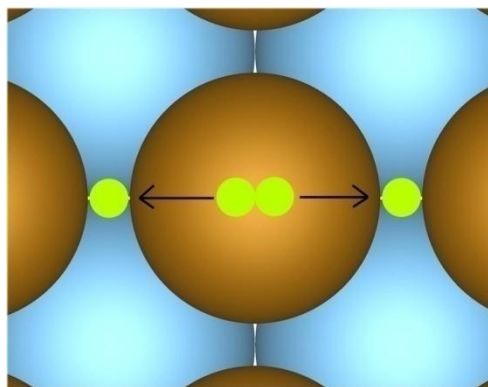


Figure 3.1 Dissociation path for the H_2 molecule over either Fe or Ti terminated (001) surfaces.

In Fe-terminated (111) surface, bridge and FCC hollow sites are the most favorable for atomic hydrogen adsorption. Although the bridge site is slightly more stable, the large difference between these two sites and other two, top and HCP hollow, confirms taking both of these sites as favorable adsorption sites for hydrogen atom adsorption. The top [2:] site for horizontal H_2 molecule is the most stable adsorption site with a very negative value in the order of eV. Here, unlike the (001) surface the rotation of hydrogen atom on top site seems to change the adsorption energy appreciably. Analyzing the dynamics of the relaxation behavior of this special site (top [2:]), one can see that the underlying layers play a major role. In the case that each hydrogen atom in the molecule points to unlike metal atoms at the sub layers (Ti in the second and Fe in the third layer as in top [2:] site which constitutes a horizontal mirror symmetry with the H_2 axis), H_2 is pulled by the surface strongly in a tilted fashion, thus an energetically stable and more favorable adsorption site appears. While in the top [1:] position there is vertical mirror symmetry, so either side of the molecule experiences the same electronic field. The molecule, then just moves a little far from the surface, which leads to a less favorable adsorption site. The bridge [1:] site has the same horizontal mirror symmetry as mentioned, which again gives rise to lower adsorption energy. In these two sites, top [2:] and bridge [1:] in Fe terminated (111) surface, the tilting of the molecule is so appreciable that the H_2 molecule would rather be chemisorbed if not restricted to in our calculations, which implies a very low or zero activation energy for the dissociation reaction.

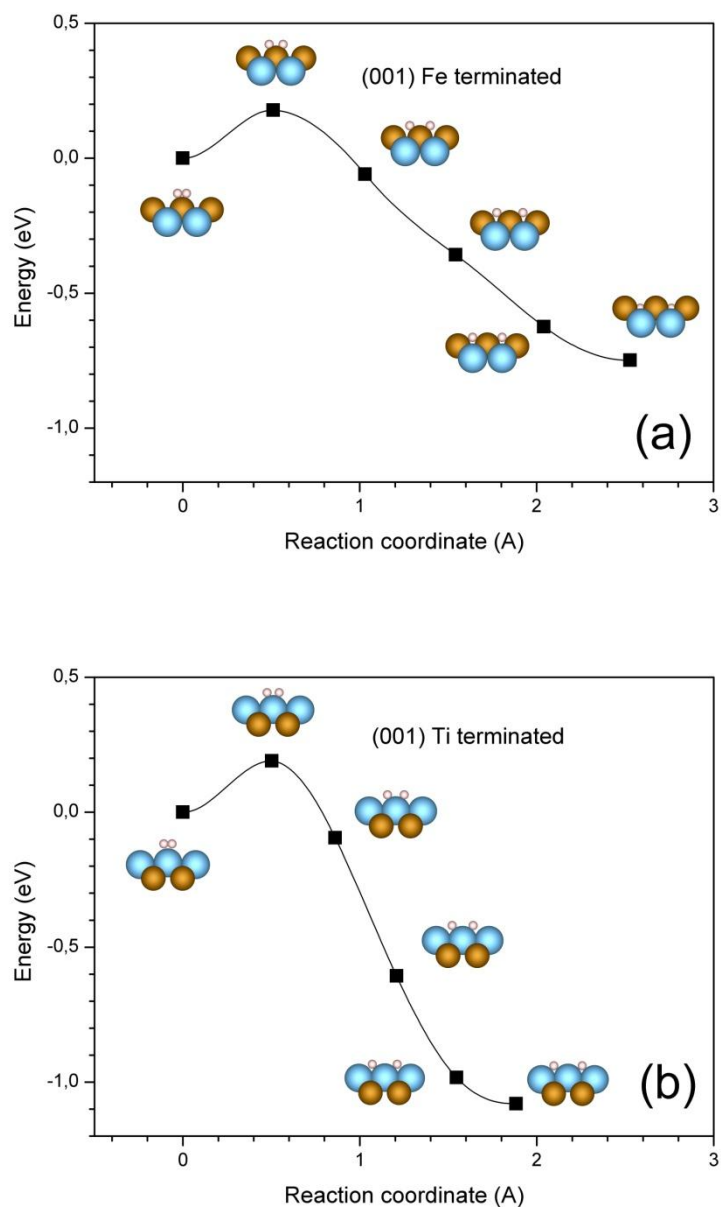


Figure 3.2 Minimum energy path (MEP) for the dissociation of H₂ molecule over (a) Fe terminated and (b) Ti terminated (001) surfaces.

We can then, represent two paths for hydrogen dissociation on this surface. In the first suggestion, Fig. (3.3a), the hydrogen molecule starts to dissociate on the top [2:] site and both hydrogen atoms follow a path, which leads them to two nearest bridge sites. Although this travelling line is not along the initial molecule axis, expresses a reasonable atom migration path. The second idea suggests that one of the hydrogen atom travels along the molecule axis until it reaches the FCC hollow site, while the other atom goes to the

nearest bridge site, Fig. (3.3b). Because of the difficulty in identification of the exact initial and final ground states of the dissociative adsorption reaction, CI-NEB calculations on this surface couldn't be performed.

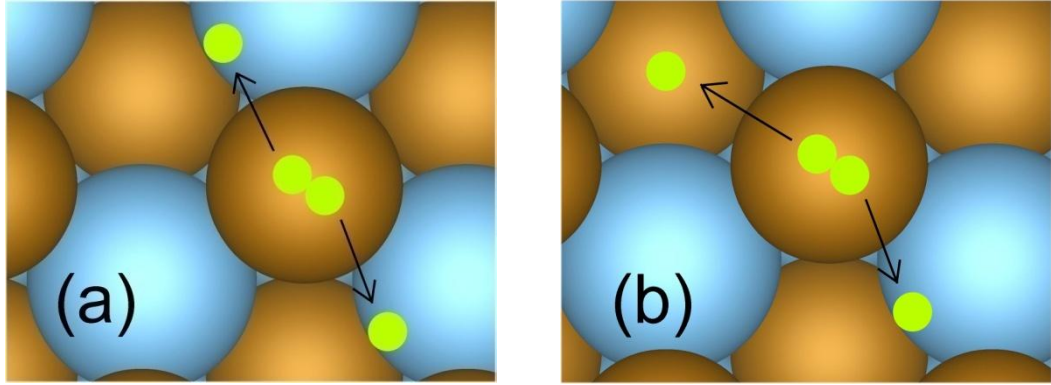


Figure 3.3 Dissociation path for the H_2 molecule over Fe terminated (111) surface. (a) First and (b) second probable paths.

In Ti-terminated (111) surface, favorable adsorption sites for atomic hydrogen came out to be bridge and HCP hollow sites. Again the bridge site shows itself a better adsorption point. Top site is the best site for molecule adsorption. However here, unlike the Fe-terminated (111) surface, the adsorption energy is in the order of meV rather than eV and there is no difference between top [1:] and [2:] cases. Two dissociation paths can be suggested: in the first one the hydrogen molecule begin to dissociate from top [1:] site along its axis until the two hydrogen atoms reach two bridge sites, Fig. (3.4a). This mechanism is more like the dissociation on (001) surface. In the second condition, dissociation starts from top [2:] site. The hydrogen atom which is near a HCP hollow site, finds its way directly to that site while the other one reaches the nearest bridge site, Fig. (3.4b). It is interesting to note that, in (001) surface the Ti-terminated surface top sites are more stable than Fe-terminated ones, but in (111) surface the result is vice versa. To ascertain that this is indeed the case, we performed Bader charge density analysis [53] on the hydrogen atoms of the adsorbed molecule. Bader analysis is a method for determining the partial charges on each atom by dividing the space into regions with surfaces that run through the saddle points in the charge density. In order to calculate the Bader charges the code developed by Henkelman [54] was used. The results show that, the charge gain of hydrogen atoms, with respect to its electronic configuration, in Ti-terminated (001) surface is more than that of Fe-terminated surface, 0.202 eu and 0.126 eu charge, respectively. This

means a stronger bond between hydrogen molecule and surface in Ti-terminated (001) surface rather than Fe-terminated (001) surface and therefore causes a more stable adsorption site. In (111) surface; however, hydrogen gains more charge in Fe-terminated surface compared to Ti-terminated, 0.168 eu and 0.035 eu, respectively. So here, unlike (001) surface, the bond between hydrogen atom and surface is more stable in Fe-terminated (111) surface.

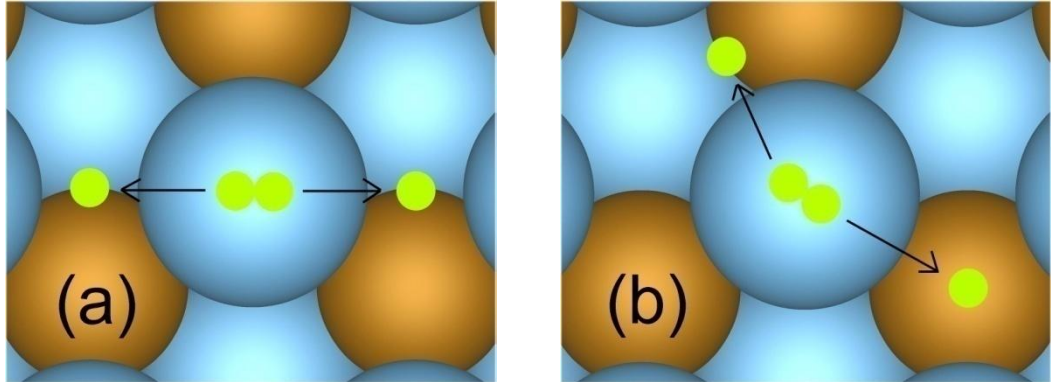


Figure 3.4 Dissociation path for the H₂ molecule over Ti terminated (111) surface. (a) First and (b) second probable paths.

In FeTi (110) surface, the best sites for adsorbing hydrogen atom seem to be 3-fold (Ti-Ti)_S-Fe hollow and Fe-Fe bridge sites. The former site is more desirable since it has lower adsorption energy. Unlike the other surfaces of FeTi which have been studied earlier, here the top site is not the most favorable point for hydrogen molecule adsorption, but the 3-fold (Ti-Ti)_L-Fe hollow [2:] site has the minimum adsorption energy. Then comes the Fe top [3:] and Fe top [2:] sites. Like the top site in Fe-terminated (111) surface, the elongation of hydrogen molecule changes the amount of adsorption energy to some extent. By rotating from position top [1:] to top [3:], the adsorption energy decreases by 10 meV. This is not quite valid for the Ti top sites. Similar to Ti-terminated (111) surface, the rotation of hydrogen molecule changes the adsorption energy only slightly and the magnitude of the adsorption energy is almost three times lower than that of Fe top sites. Considering the molecule on its most desirable adsorption site, which is 3-fold (Ti-Ti)_L-Fe hollow [2:], one of the atoms is almost already in Fe-Fe bridge site. The other atom can go either to the far side Fe-Fe bridge or Fe-Ti bridge or 3-fold (Ti-Ti)_S-Fe site, Fig. (3.5a). The other dissociation path is a simple separation of both hydrogen atoms along the molecule axis on opposite directions so that the molecule on its second favorable site, Fe top [3:], dissociates into two atoms on their most likable 3-fold (Ti-Ti)_S-Fe hollow site, Fig. (3.5b).

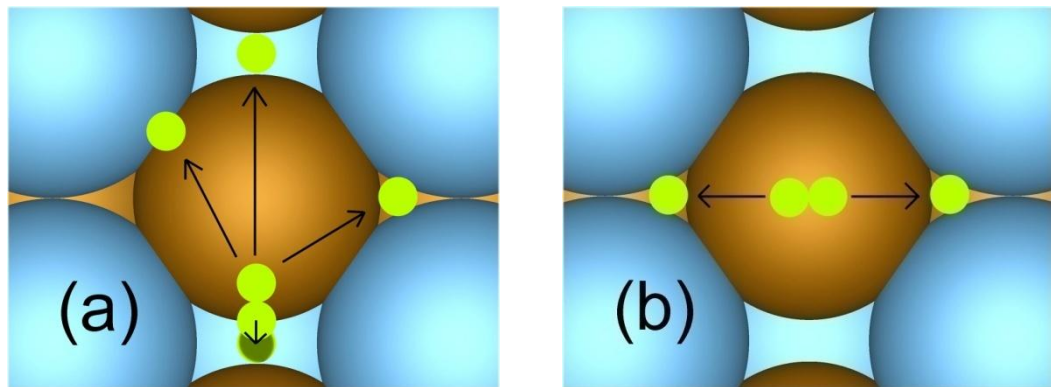


Figure 3.5 Dissociation path for the H_2 molecule over (110) surface. (a) First and (b) second probable paths.

3.2 Alloyed surfaces

3.2.1 Surface structure, relaxation and reconstruction

Relaxation behavior of the alloyed FeTi surfaces are given in Fig. (3.6), where the change in the vertical position (along the z - axis) of the alloying elements and the nearest neighbor iron and titanium atoms after substitution can be seen. For the alloying element, Δz is defined as the difference between height (z -coordinate value) of the element after relaxation and the height of the replaced Fe or Ti atom in the relaxed pure surface. Therefore, the positive values of Δz mean, rising of the atom out of the surface, whereas the negative values represent the penetration of it into the slab with respect to the pure surface.

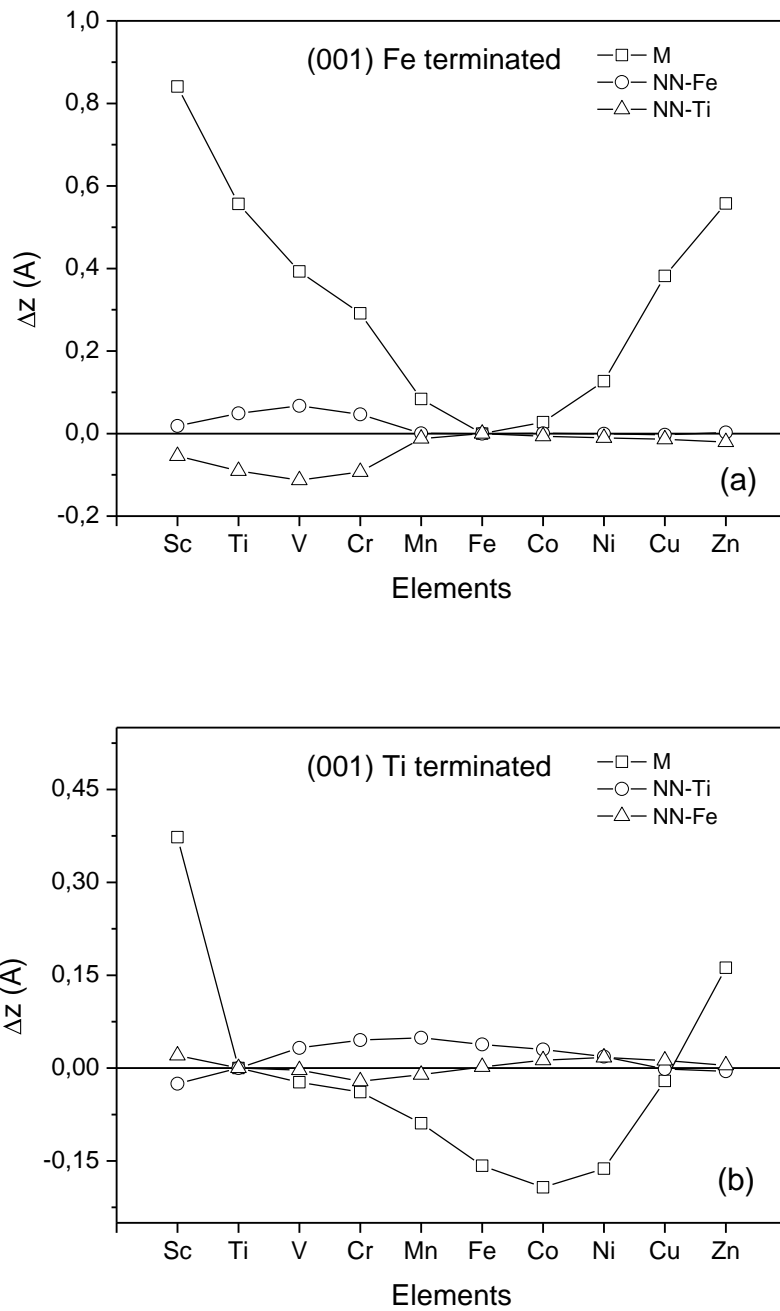


Figure 3.6 Relaxation of the top layer alloying element and nearest neighbor Fe and Ti atoms due to substitutional alloying of (a) Fe terminated (001), (b) Ti terminated (001), (c) Fe substituted (110), (d) Ti substituted (110), (e) Fe terminated (111) and (f) Ti terminated (111) surfaces. M represents the alloying element. NN-Fe and NN-Ti represents next nearest Fe and next nearest Ti atoms to alloying element, respectively.

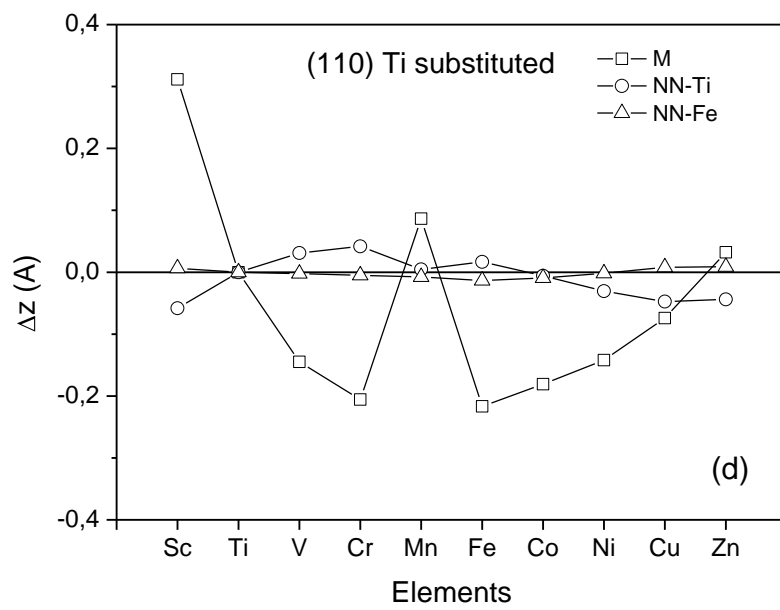
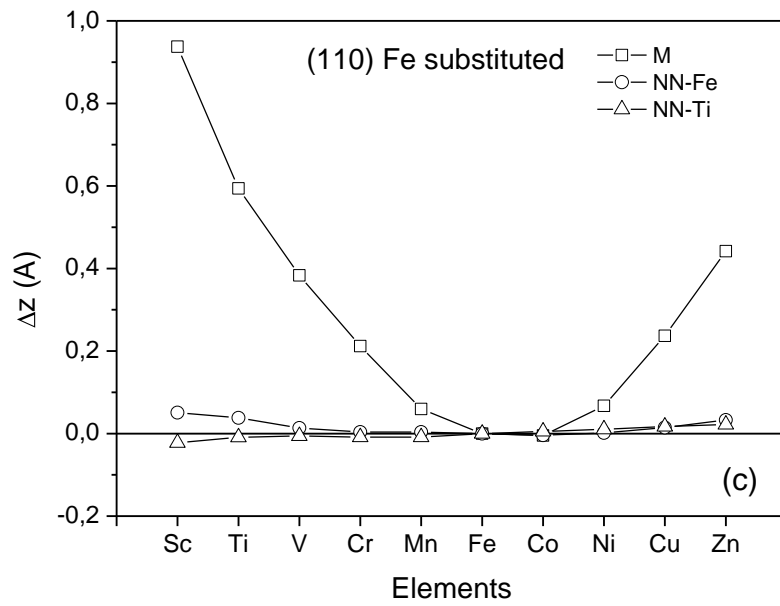


Figure 3.6 Continued.

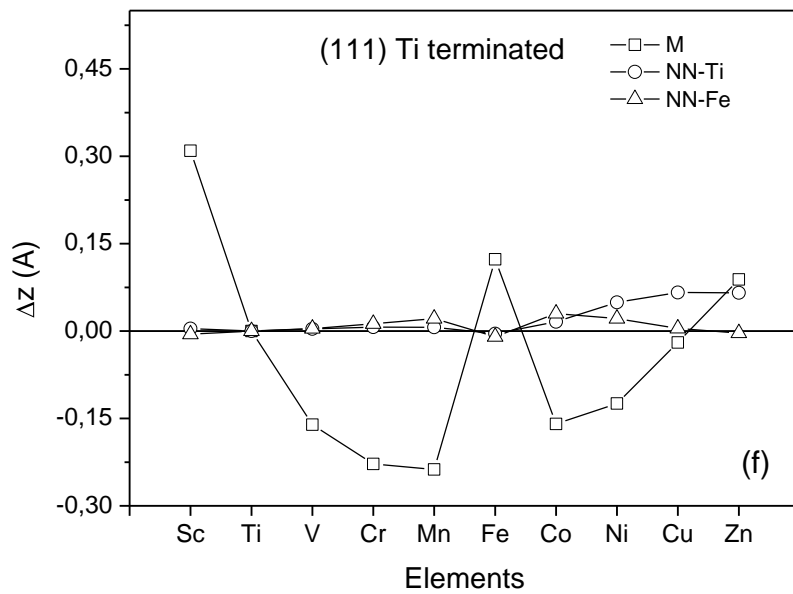
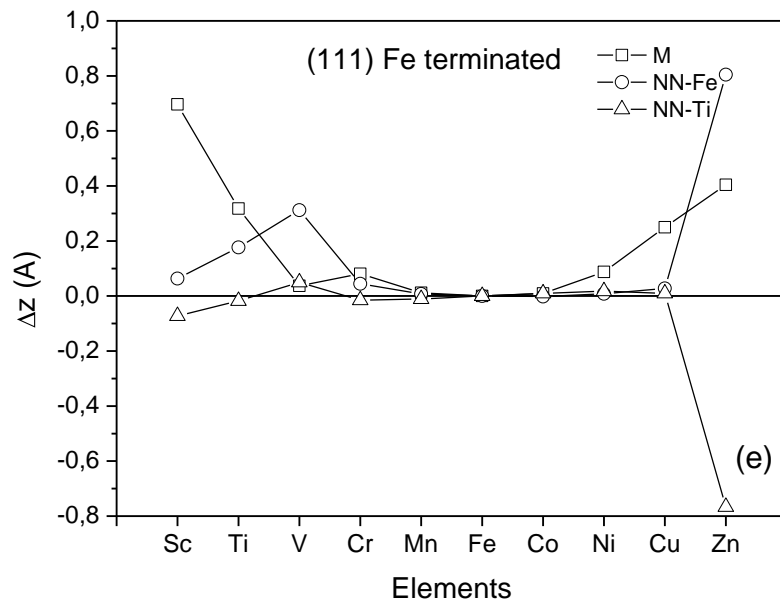


Figure 3.6 Continued.

In all of the Fe- terminated surfaces the value of Δz is always positive which means that by substitutional alloying of the Fe-terminated surfaces of FeTi, these elements move out of the surface. The more one goes far from iron in the periodic table, whether to the left or right, the more coming out of the surface appears. Therefore, the more relaxation can be

seen for elements like Sc, Ti and Zn and the least for Mn, Co and Ni. The z-coordinates of nearest neighbor iron and titanium atoms are not significantly changed in (001) and (110) surfaces compared to that of alloying element atoms. But in Fe-terminated (111) surface where the layers are so close to each other, there is somewhat more relaxation. In addition, a general rule can be devised that, in Fe-terminated surfaces, if neighboring iron atoms are elevated from the surface then titanium atoms in the sub layer go slightly further inside the slab.

Except the first and the last elements of the 3d metals, others penetrate into the surface in Ti-terminated FeTi surfaces. There is a kind of symmetry in Δz versus alloying elements curves where middle elements experience more penetration into the surface. Co in (001), Fe in (110) and Mn in (111) are the elements cause most relaxation in mentioned surfaces. However, in (110) and (111) surfaces Mn and Fe, respectively, express a spike from the surface instead of going into it. Nearest neighbor Fe and Ti also relax slightly in the Ti-terminated surfaces.

Fig. (3.7) shows the change in distance between the nearest neighbor Fe or Ti and the alloying element, before and after substituting the alloying element. So Δr , in percentage, is the change in the radial spacing between the replaced Fe or Ti atom and the nearest neighbor Fe or Ti atom after alloying. In (110) surface, both of the nearest neighbor atoms are at the topmost surface layer, however in (001) and (111) surfaces, because of the different terminations one of them resides at the topmost layer and the other one on the second layer from the surface. So positive Δr means repulsion between nearest neighbor atom and the substituent alloying atom and negative Δr means attraction between them. As can be seen, considerable amount of reconstruction happens in all cases.

In Fe-terminated (001) and (111) and Fe substituted (110), the nearest neighbor Fe atom is being attracted to the substituent alloying element and nearest neighbor Ti is repulsed. The more powerful attraction forces between replaced alloying elements and nearest neighbor Fe can be seen in elements on the right side of Fe in periodic table. Here, V shows the most attracted element to Fe on these surfaces. The more one goes far from Fe in the periodic table (e.g. Sc, Ti and Zn), the amount of repulsion between the alloying element and nearest neighbor Ti increases.

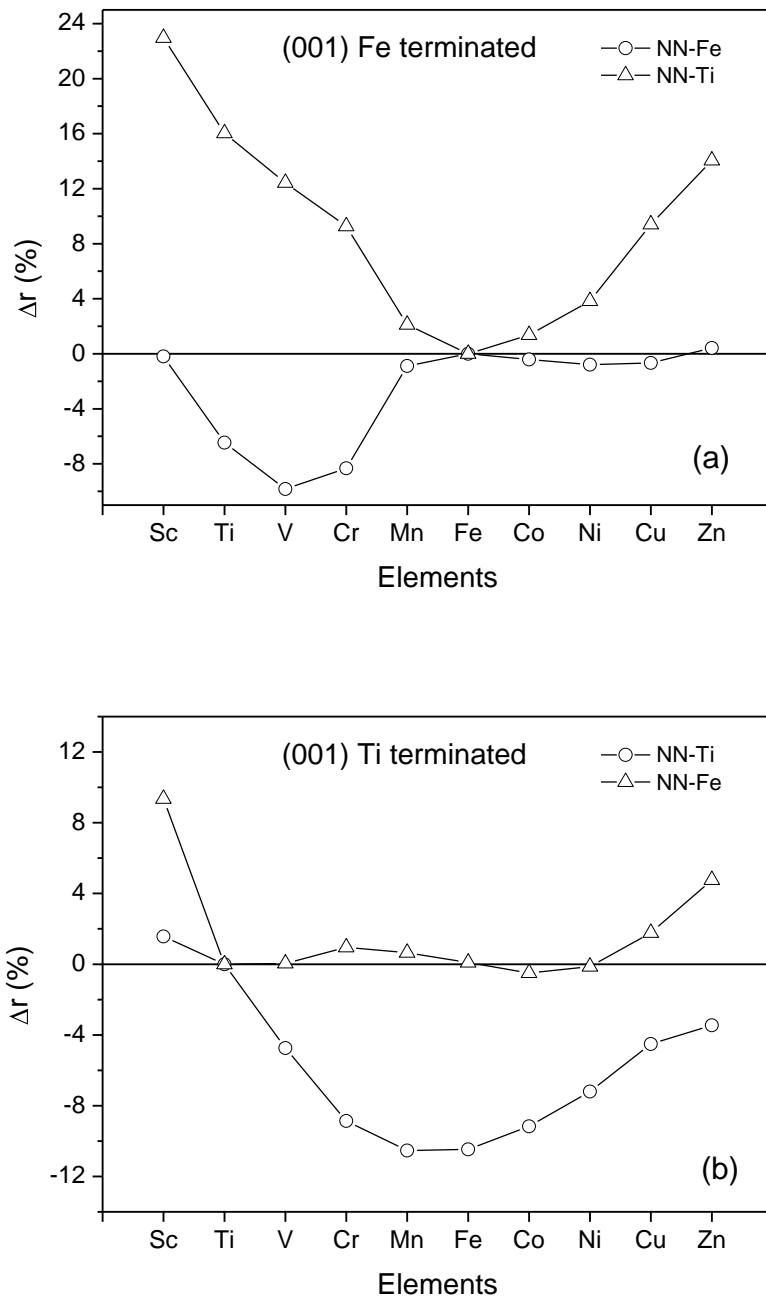


Figure 3.7 Reconstruction of the top layer Fe and Ti atoms that are nearest neighbors to the alloying element, due to substitutional alloying of (a) Fe terminated (001), (b) Ti terminated (001), (c) Fe substituted (110), (d) Ti substituted (110), (e) Fe terminated (111) and (f) Ti terminated (111) surfaces. NN-Fe and NN-Ti represents next nearest Fe and next nearest Ti atoms to alloying element, respectively.

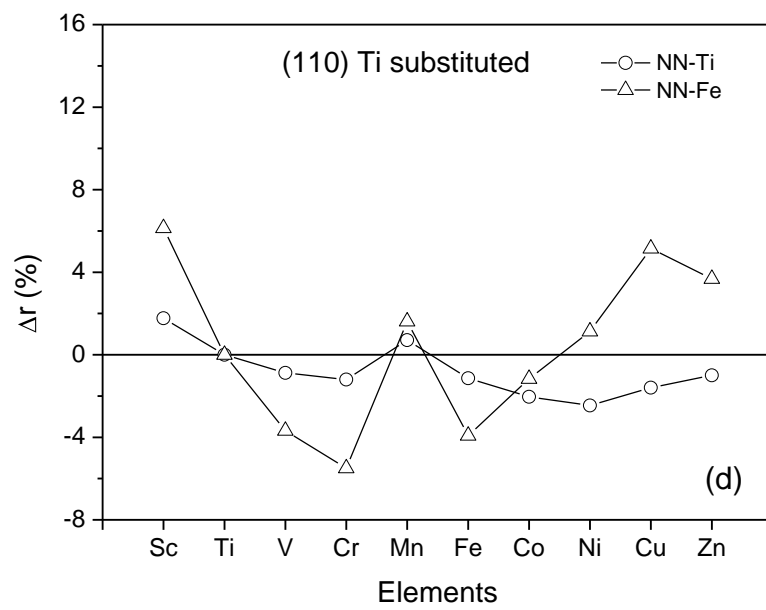
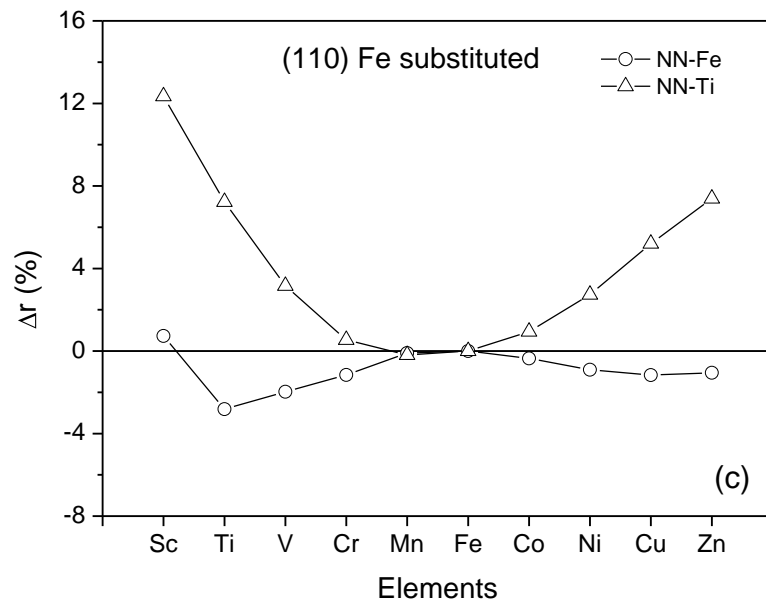


Figure 3.7 Continued.

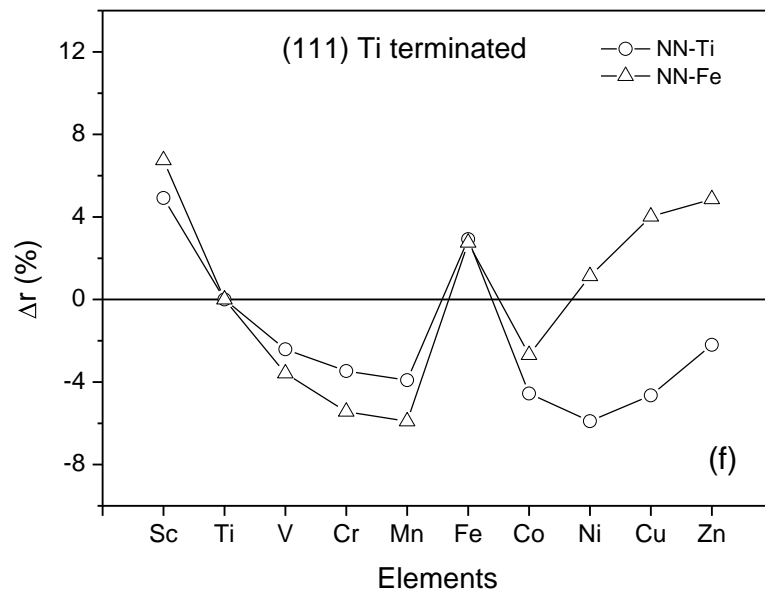
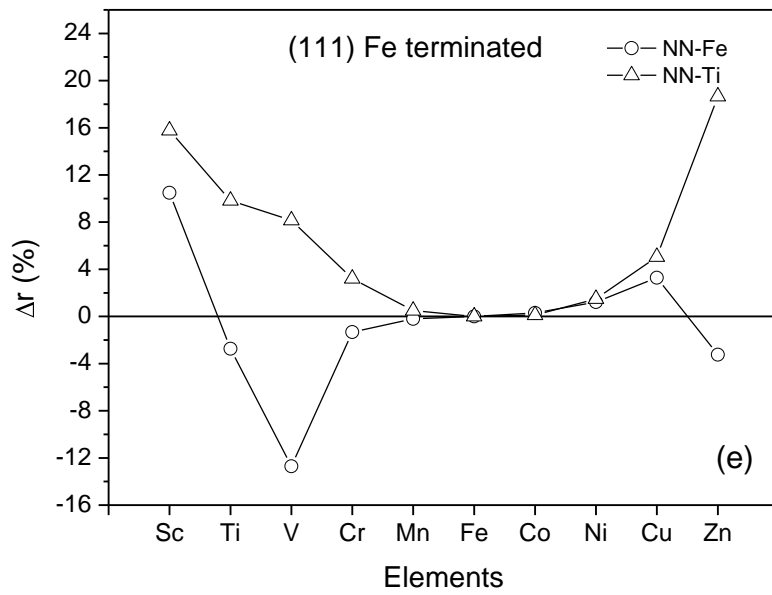


Figure 3.7 Continued.

In general, the radial spacing between alloying elements and nearest neighbor Ti decreases for both Ti-terminated (001) and (111) surfaces. The radial spacing for the nearest neighbor Fe; however, only slightly varies in Ti-terminated (001) surface. On the

other hand, in Ti-terminated (111) surface, both Fe and Ti as nearest neighbor atoms, have a similar behavior, except for Ni, Cu and Zn in which Ti attracts the replacing alloying element while Fe goes further away. Reconstruction pattern for Ti-substituted (110) surface is mostly like that of Ti-terminated (111) surface.

3.2.2 Substitutional adsorption energy of alloying elements

The substitutional adsorption energies of alloying elements are calculated using Eq. (2.5). As it was mentioned in Section (2.2.2), two different energy terms should be calculated in order to reach the adsorption energy: Energy for the isolated atoms and step formation energy. In order to calculate the latter, for (001) and (111) surfaces, high symmetry step sites over them should be determined and the one that has the minimum in adsorption energy must be considered as the most favorable step site for the respective surface structure. We decided these sites to be top, bridge and hollow sites as mentioned earlier. For (110) surface which shows no termination, this step site is simply the regular lattice position over the surface. The calculated step formation energies are shown in Table (3.3).

Table 3.3 Step formation energies for FeTi surfaces. The most stable sites are shown in bold font.

Surface	High symmetry kink site	Step formation energy (eV)
(001) Fe-terminated	Top	-4.62
	Bridge	-5.79
	4-fold Hollow	-6.86
(001) Ti-terminated	Top	-6.16
	Bridge	-6.58
	4-fold Hollow	-7.25
(111) Fe-terminated	Top	-5.05
	Bridge	-9.63
	3-fold FCC Hollow	-9.64
	3-fold HCP Hollow	-6.66
(111) Ti-terminated	Top	-3.08
	Bridge	-6.96
	3-fold FCC Hollow	-6.97
	3-fold HCP Hollow	-6.62
(110) Fe substituted	-	-6.71
(110) Ti substituted	-	-8.12

The favorable step sites came out to be the four-fold hollow sites for (001) and FCC hollow sites for (111) surfaces in both terminations. Hence, the adsorption energy for alloying elements of 3d transition metals on all surfaces are calculated and presented in Table (3.4). The results are represented graphically in Fig. (3.8).

Table 3.4 The substitutional adsorption energies, in (eV), for 3d alloying elements on all surfaces.

	(100) Fe	(100) Ti	(111) Fe	(111) Ti	(110) Fe	(110) Ti
Sc	-4.24	-4.58	-6.55	-3.84	-2.72	-4.58
Ti	-4.49	-	-6.79	-	-3.37	-
V	-3.59	-4.63	-6.07	-3.85	-2.93	-5.22
Cr	-1.47	-3.03	-4.11	-1.67	-1.34	-3.13
Mn	-1.77	-3.28	-4.69	-1.40	-1.89	-2.23
Fe	-	-4.55	-	-1.60	-	-3.58
Co	-7.98	-8.93	-10.80	-6.31	-7.75	-7.68
Ni	-4.27	-5.29	-7.29	-2.66	-4.00	-4.10
Cu	-2.83	-3.64	-5.82	-1.55	-2.30	-2.89
Zn	-1.06	-1.71	-3.80	-0.19	-0.27	-1.33

In all of the surfaces studied, a similar behavior is seen in the adsorption energies of the alloying elements. As going from early to late transition metals in the 3d series, substitutional adsorption energy of the elements initially increases slightly making the adsorption process less favorable. This is especially apparent for Cr, Mn and/or Fe. Then there is a sharp decrease in the adsorption energy when the substituent element becomes Co. After that, it starts to rise and the system becomes less stable again. Therefore, Co is considered to make the most stable bonds with FeTi surfaces, regardless of surface index or termination, and hence is the most suitable alloying element to replace one of the FeTi surface atoms.

On the other hand, comparing surfaces together, Fe-terminated (111) surface shows the most negative adsorption energy and therefore is the best surface for adsorbing alloying elements substitutionally. However, Ti-terminated (111) surface shows the highest value of adsorption energy and therefore the least stable surface structure with alloying elements.

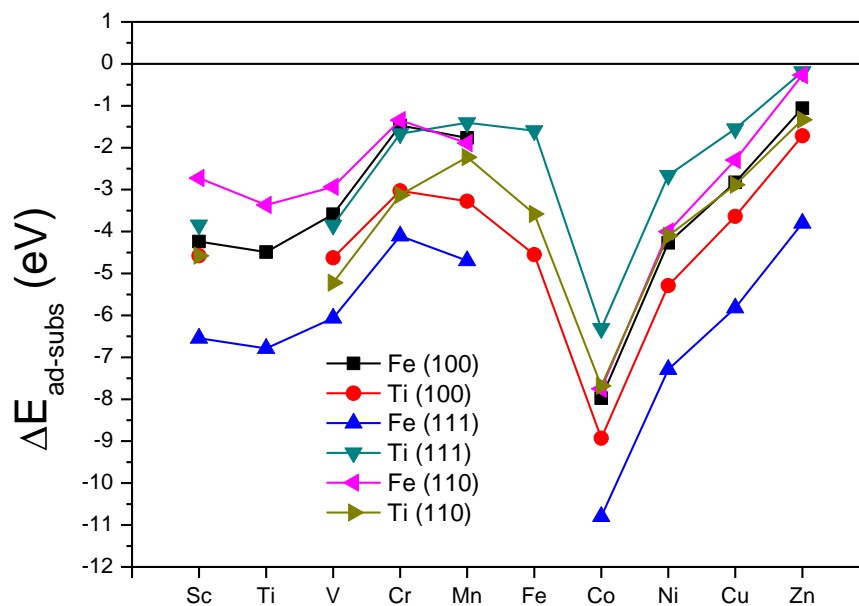


Figure 3.8 The substitutional adsorption energies for 3d alloying elements on all surfaces.

As a discussion, since the 3d orbital of Co, Fe and Ni are most unbounded, these elements show a powerful affinity to build a bond with Fe and Ti atoms in order to fulfill their orbital with pair electrons in each one and reach the minimum energy level hence the maximum stability. So the adsorption energies of these elements are minimum in almost all the surfaces. On the other hand, Zn is the most stable element among 3d series (because of its full 3d orbital) and it shows the least desire to substitute surface atoms. Therefore, its adsorption energy is highest in all the surfaces.

CHAPTER 4

CONCLUSIONS

In this study, dissociation of hydrogen on three low index surfaces of FeTi was computationally investigated using density functional theory within generalized gradient approximation. After testing the package code VASP for accuracy of theoretical predictions by comparing the calculated and experimental lattice constants, adsorption energies of molecular and atomic hydrogen on Fe- and Ti- terminated FeTi (001), Fe- and Ti-terminated FeTi (111) and FeTi (110) surfaces were calculated on high symmetry adsorption sites.

The most stable sites for the molecular hydrogen came out to be top sites in (001) and (111) surfaces, whereas in (110) surface top site is the second favorable. The most stable site for H₂ in (110) was found to be the 3-fold hollow site which is composed of a long Ti-Ti bridge and an Fe atom. Calculated adsorption energies for the top sites in Fe-terminated (001), Ti-terminated (001), Fe-terminated (111), Ti-terminated (111) and (Ti-Ti)_L-Fe (110) were -0.463, -0.917, -2.231, -0.151 and -0.599 eV/H₂, respectively. Meanwhile, the most favorable adsorption sites for atomic hydrogen were determined as bridge sites in all terminated (001) and (111) surfaces. The adsorption energies were -2.863, -3.526, -4.504 and -3.140 eV/H for Fe-terminated (001), Ti-terminated (001), Fe-terminated (111) and Ti-terminated (111), respectively. In (110) surface, 3-fold (Ti-Ti)_S-Fe hollow site is the most favorable site for hydrogen atom adsorption.

Considering molecular and atomic hydrogen adsorption sites, the most likely paths of hydrogen molecule dissociation on different surfaces of FeTi were predicted. Also, using CI-NEB method, the dissociation reaction path and activation energy for (001) surfaces was calculated. The activation energies came out to be 0.178 and 0.190 eV for Fe- and Ti-terminated (001) surfaces, respectively. On Fe-terminated (111) and FeTi (110) surfaces however, the dissociation of hydrogen molecule happens readily without any activation barrier.

Secondly, we have calculated the substitutional adsorption energies of 3d transition metals for each surface. Among all the surfaces, Fe-terminated (111) surface came out to be the most favorable one. In addition, Co had the lowest adsorption energy in all surfaces and therefore was the best substitutionally adsorbed alloying element. Zn and Cr/Mn, on the other hand, show the least desire to be adsorbed on all the surfaces.

REFERENCES

1. R. P. Dahia, *Progress in Hydrogen Energy* (D. Reidel Publishing Company, 1987).
2. A. Zuttel, A. Borgschulte, and L. Schlapbach, *Hydrogen as a Future Energy Carrier* (Wiley-VCH, 2008).
3. H. Hiller and R. Reimert, *Gas Production*, Vol. A12, 5 ed. (Ullmann's Encyclopedia of Industrial Chemistry, 2000).
4. R. Hino and X. L. Yan, in *Hydrogen Fuel, Production, Transport and Storage*, edited by R. B. Gupta (CRC Press, 2009).
5. D. A. Bechrakis and E. Varkaraki, in *Hydrogen Fuel, Production, Transport and Storage*, edited by R. B. Gupta (CRC Press, 2009).
6. N. G. Dhere and R. S. Bennur, in *Hydrogen Fuel, Production, Transport and Storage*, edited by R. B. Gupta (CRC Press, 2009).
7. W. De Jong, in *Hydrogen Fuel, Production, Transport and Storage*, edited by R. B. Gupta (CRC Press, 2009).
8. A. Damle, in *Hydrogen Fuel, Production, Transport and Storage*, edited by R. B. Gupta (CRC Press, 2009).
9. M. Gao and R. Krishnamurthy, in *Hydrogen Fuel, Production, Transport and Storage*, edited by R. B. Gupta (CRC Press, 2009).
10. K. K. Pant and R. B. Gupta, in *Hydrogen Fuel, Production, Transport and Storage*, edited by R. B. Gupta (CRC Press, 2009).
11. H. Li, M. Eddaoudi, M. O'Keeffe, and O. M. Yaghi, *Nature* **402**, 276 (1999).
12. D. Grant, in *Solid-State Hydrogen Storage Materials and Chemistry*, edited by G. Walker (CRC Press, 2008).
13. C. Jensen, Y. Wang, and M. Y. Chou, in *Solid-State Hydrogen Storage Materials and Chemistry*, edited by G. Walker (CRC Press, 2008).
14. Y. Nakamori and S. Orimo, in *Solid-State Hydrogen Storage Materials and Chemistry*, edited by G. Walker (CRC Press, 2008).
15. D. H. Gregory, in *Solid-State Hydrogen Storage Materials and Chemistry*, edited by G. Walker (CRC Press, 2008).

16. J. Hafner, *J. Comput. Chem.* **29**, 2044 (2008).
17. R. Car, *Quant. Struct. -Act. Relat.* **21**, 97 (2002).
18. P. Atkins and J. De Paula, *Atkin's Physical Chemistry*, 7 ed. (Oxford University Press, 2002).
19. R. Yang, Y. M. Wang, Y. Zhao, L. B. Wang, H. Q. Ye, and C. Y. Wang, *Acta Mater.* **50**, 109 (2002).
20. N. Nishimiya, T. Wada, A. Matsumoto, and K. Tsutsumi, *J. Alloys Compds.* **313**, 53 (2000).
21. Y. Song, Z. X. Guo, and R. Yang, *Mater. Sci. Eng. A* **365**, 73 (2004).
22. C. Wolverton, D. J. Siegel, A. R. Akbarzadeh, and V. Ozolins, *J. Phys. Condens. Matter.* **20**, 064228 (2008).
23. A. Kinaci and M. K. Aydinol, *Int. J. Hydrogen Energy* **32**, 2466 (2007).
24. A. Zuttel, *Naturwissenschaften* **91**, 157 (2004).
25. G. Lee, J. S. Kim, Y. M. Koo, and S. E. Kulkova, *Int. J. Hydrogen Energy* **27**, 403 (2002).
26. I. N. Yakovkin, *Surf. Sci.* **577**, 229 (2005).
27. D. E. Jiang and E. A. Carter, *Surf. Sci.* **570**, 167 (2004).
28. H. T. Chen, D. G. Musaev, and M. C. Lin, *J. Phys. Chem. C* **111**, 17333 (2007).
29. S. Banerjee, C. G. S. Pillai, and C. Majumder, *J. Chem. Phys.* **129**, 174703 (2008).
30. H. F. Busnengo and A. E. Martinez, *J. Phys. Chem. C* **112**, 5579 (2008).
31. D. Kecik and M. K. Aydinol, *Surf. Sci.* **603**, 304 (2009).
32. P. E. Blöchl, *Phys. Rev. B* **50**, 17953 (1994).
33. G. Kresse and J. Furthmuller, *Comp. Mat. Sci.* **6**, 15 (1996).
34. G. Kresse and J. Furthmuller, *Phys. Rev. B* **54**, 11169 (1996).
35. G. Kresse and J. Hafner, *Phys. Rev. B* **47**, 558 (1993).

36. G. Kresse and D. Joubert, *Phys. Rev. B* **59**, 1758 (1999).
37. J. P. Perdew, K. Burke, and M. Ernzerhof, *Phys. Rev. Lett.* **77**, 3865 (1996).
38. P. Thompson, J. J. Reilly, and J. M. Hastings, *J. Appl. Crystallogr.* **22**, 256 (1989).
39. P. Thompson, M. A. Pick, F. Reidinger, L. M. Corliss, J. M. Hastings, and J. J. Reilly, *J. Phys. F* **8**, L75 (1978).
40. P. Fischer, J. Schefer, K. Yvon, L. Schlapbach, and T. Riesterer, *J. Less-Common Met.* **129**, 39 (1987).
41. J. J. Reilly and R. H. Wishwall, *Inorg. Chem.* **13**, 218 (1974).
42. M. Methfessel and A. T. Paxton, *Phys. Rev. B* **40**, 3616 (1989).
43. Y. Song, Z. X. Guo, and R. Yang, *Phys. Rev. B* **69**, 094205 (2004).
44. T. Vegge, L. S. Hedegaard-Jensen, J. Bonde, T. R. Munter, and J. K. Norskov, *J. Alloys Compds.* **386**, 1 (2005).
45. D. M. Bird, L. J. Clarke, M. C. Payne, and I. Stich, *Chem. Phys. Lett.* **212**, 518 (1993).
46. A. J. Du, S. C. Smith, X. D. Yao, and G. Q. Lu, *Surf. Sci.* **600**, 1854 (2006).
47. M. Tsuda, W. A. Dino, H. Kasai, H. Nakanishi, and H. Aikawa, *Thin Solid Films* **509**, 157 (2006).
48. G. Wu, J. Zhang, Y. Wu, Q. Li, K. Chou, and X. Bao, *Acta Phys. -Chim. Sin.* **24**, 55 (2008).
49. G. Henkelman and H. Jonsson, *J. Chem. Phys.* **113**, 9978 (2000).
50. G. Henkelman, B. P. Uberuaga, and H. Jonsson, *J. Chem. Phys.* **113**, 9901 (2000).
51. D. Shepherd, R. Terrel, and G. Henkelman, *J. Chem. Phys.* **128**, 134106 (2008).
52. A. S. Pedersen, P. J. Moller, and O. T. Sorensen, *Physica Scripta* **T4**, 83 (1983).
53. R. F. W. Bader, *Atoms in Molecules* (Clarendon Press, 1990).
54. G. Henkelman, A. Arnaldsson, and H. Jonsson, *Comput. Mater. Sci.* **36**, 254 (2006).